HHS Public Access

Author manuscript

Dev Cell. Author manuscript; available in PMC 2019 May 11.

Published in final edited form as:

Dev Cell. 2019 February 11; 48(3): 329–344.e5. doi:10.1016/j.devcel.2018.11.035.

SPOP Promotes Nanog Destruction to Suppress Stem Cell Traits and Prostate Cancer Progression

Jinfang Zhang[#1], **Ming Chen**[#2,9], **Yasheng Zhu**[#3], **Xiangpeng Dai**[1], **Fabin Dang**[1], **Junming Ren**[1], **Shancheng Ren**[3], **Yulia V. Shulga**[2], **Francisco Beca**[1,11], **Wenjian Gan**[1], **Fei Wu**[1,4], **Yu-Min Lin**[5], **Xiaobo Zhou**[6,7], **James A. DeCaprio**[8], **Andrew H. Beck**[1], **Kun Ping Lu**[5], **Jiaoti Huang**[9], **Cheryl Zhao**[10], **Yinghao Sun**[3], **Xu Gao**[3,*], **Pier Paolo Pandolfi**[2,*], and **Wenyi Wei**[1,13,*]

[1]Department of Pathology, Beth Israel Deaconess Medical Center, Harvard Medical School, Boston, MA 02215, USA

[2]Cancer Research Institute, Beth Israel Deaconess Cancer Center, Department of Medicine and Pathology, Beth Israel Deaconess Medical Center, Harvard Medical School, Boston, MA 02215, USA

[3]Department of Urology, Shanghai Changhai Hospital, Second Military Medical University, Shanghai 200433, China

[4]Department of Urology, Huashan Hospital, Fudan University, Shanghai 200040, China

[5]Division of Translational Therapeutics, Department of Medicine, Beth Israel Deaconess Medical Center, Harvard Medical School, Boston, MA 02215, USA

[6]Channing Division of Network Medicine, Brigham and Women's Hospital and Harvard Medical School, Boston, MA, USA

[7]Division of Pulmonary and Critical Care Medicine, Department of Medicine, Brigham and Women's Hospital and Harvard Medical School, Boston, MA, USA

[8]Department of Medical Oncology, Dana-Farber Cancer Institute and Department of Medicine, Brigham and Women's Hospital, Harvard Medical School, Boston, MA 02215, USA

[9]Department of Pathology, Duke University School of Medicine, Durham, NC 27710, USA

[10]Stemmera Inc, 3475 Edison Way Suite J2, Menlo Park, CA 94025, USA

[11]Department of Pathology, Stanford University School of Medicine, Stanford, CA 94305-5324, USA

[*]Correspondence: gaoxu.changhai@foxmail.com (X.G.), ppandolf@bidmc.harvard.edu (P.P.P.), wwei2@bidmc.harvard.edu (W.W.).

AUTHOR CONTRIBUTIONS

J.Z., M.C., and Y.Z. performed most of the experiments with help from X.D., F.D., J.R., S.R., Y.V.S., W.G., F.W., Y.-M.L., J.A.D., K.P.L, J.H., C.Z., and Y.S. J.Z., M.C., and W.W. designed experiments. J.Z. and W.W. wrote the manuscript. Y.Z., S.R., X.G., and Y.S. performed the immunohistochemistry (IHC) assays. F.B. and A.H.B. performed the bioinformatics analysis. W.W., P.P.P., and X.G. guided and supervised the project. All authors commented on the manuscript.

[13]Lead Contact

SUPPLEMENTAL INFORMATION

Supplemental Information includes six figures and one table and can be found with this article online at https://doi.org/10.1016/j.devcel.2018.11.035.

DECLARATION OF INTERESTS

The authors declare no competing interests.

[#] These authors contributed equally to this work.

SUMMARY

Frequent *SPOP* mutation defines the molecular feature underlying one of seven sub-types of human prostate cancer (PrCa). However, it remains largely elusive how SPOP functions as a tumor suppressor in PrCa. Here, we report that SPOP suppresses stem cell traits of both embryonic stem cells and PrCa cells through promoting Nanog poly-ubiquitination and subsequent degradation. Mechanistically, Nanog, but not other pluripotency-determining factors including Oct4, Sox2, and Klf4, specifically interacts with SPOP via a conservative degron motif. Importantly, cancer-derived mutations in *SPOP* or at the Nanog-degron (S68Y) disrupt SPOP-mediated destruction of Nanog, leading to elevated cancer stem cell traits and PrCa progression. Notably, we identify the Pin1 oncoprotein as an upstream Nanog regulator that impairs its recognition by SPOP and thereby stabilizes Nanog. Thus, Pin1 inhibitors promote SPOP-mediated destruction of Nanog, which provides the molecular insight and rationale to use Pin1 inhibitor(s) for targeted therapies of PrCa patients with wild-type *SPOP*.

In Brief

Zhang et al. show that the Cullin 3/SPOP E3 ligase regulates prostate cancer stem cell traits by promoting Naong polyubiquitination and degradation. They find that cancer-derived SPOP mutations or overexpression of the Pin1 oncoprotein disrupts SPOP-mediated destruction of Nanog, leading to elevated cancer stem cell traits and prostate cancer progression.

INTRODUCTION

Prostate cancer (PrCa) is the most common cancer in males and the second leading cause of cancer-related death for men in the United States and Europe (Ferlay et al., 2013; Siegel et al., 2013). It is estimated that in 2018, PrCa will be diagnosed in 164,690 men in the United States alone and 29,430 will die of this deadly disease (Siegel et al., 2018). Whole-genome sequencing studies have revealed that genomic rearrangements and copy number aberrations are among the driving forces for prostate tumorigenesis (Baca et al., 2013; Beroukhim et al., 2010; Tomlins et al., 2008; Liu et al., 2006). Furthermore, recent systematic sequencing studies have revealed that recurrent somatic mutation at multiple susceptible genes is also a key molecular feature of human PrCa (Barbieri et al., 2012; Berger et al., 2011).

Strikingly, mutations in *SPOP* (Speckle-type POZ protein), a substrate-interacting adaptor for the Cullin 3-based E3 ubiquitin ligase complexes (Mani, 2014; Genschik et al., 2013), occur in approximately 10%–15% of primary human PrCas, representing a molecular feature for one of the seven recently categorized sub-types of PrCa (Cancer Genome Atlas Research Network, 2015). Moreover, analogous to the well-characterized mutations in *Fbw7* tumor suppressor (Wang et al., 2011; Wang et al., 2012b), *SPOP* mutations in human PrCa are largely clustered in its substrate binding MATH domain. This hotspot mutation feature is typically observed in tumor suppressor genes such as *p53* (Kamp et al., 2016; Stracquadanio et al., 2016) and *Fbw7* (Wang et al., 2014), which further indicates that SPOP loss-of-function mutations may promote tumorigenesis in part via disrupting its physiological

function toward regulating its downstream ubiquitin substrates (Barbieri et al., 2012; Berger et al., 2011).

Moreover, as most of characterized SPOP downstream substrates including androgen receptor (AR) (An et al., 2014; Geng et al., 2014), steroid receptor coactivator 3 (SRC-3) (Geng et al., 2013), DEK (Theurillat et al., 2014), TRIM24 (Theurillat et al., 2014), and ERG (An et al., 2015; Gan et al., 2015) are wellknown oncogenic proteins that are frequently overexpressed in human PrCa, SPOP probably functions as a tumor suppressor to negatively regulate the stability of these oncogenic proteins in the PrCa setting. However, in other cancer settings including kidney cancer, SPOP is, on the contrary, overexpressed and displays a possible oncogenic role in part by promoting the degradation of the PTEN tumor suppressor protein (Li et al., 2014). Thus, the physiological role of SPOP in tumorigenesis is rather tissue and cellular context dependent. Hence, this study mainly focuses on understanding the tumor suppressor role of SPOP in the PrCa setting by regulating prostate cancer stem cell (CSC) traits to govern prostate tumorigenesis process.

Nanog is initially identified as one of the key factors critical for maintaining the self-renewal ability and pluripotency of mouse embryonic stem (mES) cells (Chambers et al., 2003; Mitsui et al., 2003). However, emerging evidence suggests that Nanog has oncogenic features such as enhancing cancer cell migration and invasion (Siu et al., 2013) and is frequently upregulated in various human malignancies, contributing to carcinogenesis in part by initiating and preserving CSCs (Wong and Cheung, 2016). Targeting CSCs is considered a promising therapeutic approach to combat various types of human cancers including PrCa (Dean et al., 2005). Given that Nanog plays a pivotal role in cancer stem cell maintenance, targeting the Nanog oncoprotein, such as elevating the ubiquitin-mediated degradation event of Nanog, may eliminate CSCs to achieve better clinical outcomes (Wang et al., 2013a). However, the upstream regulatory circuit(s), especially the physiological E3 ubiquitin ligase(s) that governs Nanog protein stability still remains largely unknown.

In this study, we provide a novel molecular mechanism underlying the tumor suppressive role of SPOP in PrCa through promoting the destruction of the Naong oncoprotein to restrict CSC traits as well as provide the molecular basis for future usage of Pin1 inhibitors in treating PrCa with wild-type (WT) *SPOP* genetic makeup.

RESULTS

Cullin 3^{SPOP} Suppresses PrCa Stem Cell Traits in a Nanog-Dependent Manner

Although phosphorylation modification has been reported to control Nanog stability through ubiquitin-proteasome pathway(s) (Kim et al., 2014; Ramakrishna et al., 2011; Moretto-Zita et al., 2010), the identity of the specific E3 ligase for Nanog remains to be identified. In keeping with this notion, we found that the abundance of endogenous Nanog can be markedly elevated upon inhibiting the 26S proteasome with MG132 (Figure S1A), suggesting the involvement of ubiquitin-mediated pathways in controlling Nanog stability. Given that multi-subunit Cullin-based RING-type E3 ligase complexes (CRLs) constitute the largest family member of E3 ligases in the human genome (Zheng et al., 2016; Wang et al., 2014), we went on to explore whether MLN4924, a specific inhibitor of the NEDD8-

activating enzyme (Nawrocki et al., 2012) that inactivates all CRLs through blocking Cullin neddylation (Soucy et al., 2009), influences Nanog abundance in cells. Notably, MLN4924 elevated endogenous Nanog protein abundance at levels comparable to MG132 treatment (Figure S1A), indicating the involvement of specific yet unidentified CRL(s) in negative regulation of Nanog stability in cells.

In keeping with this notion, we further found that only Cullin 3, but not other related Cullin family members (Cullin 1, 2, 4A, 4B, 5, and 7), interacted with Nanog in cells (Figures 1A and S1B). Moreover, ectopic expression of Cullin 3, but not Cullin 7, dramatically promoted the degradation of Nanog in cells (Figure S1C), arguing that Cullin 3-based CRL, but not the Cullin 7-based E3 ligase complex, plays an important role in governing Nanog protein stability in cells. In support of this notion, we found that genetic deletion of endogenous *Cullin 7* in mouse embryonic fibroblasts (MEFs) (Ponyeam and Hagen, 2012; Sarikas et al., 2008) did not affect endogenous Nanog protein abundance (Figure S1D). On the other hand, depletion of *Cullin 3*, in PC3 or DU145 PrCa cells led to elevated abundance of endogenous Nanog (Figures 1B and S1E), providing further support for a critical physiological role of Cullin 3 in negatively regulating Nanog stability in the PrCa setting.

It has been well documented that Cullin 3 exerts its E3 ligase activity as a multi-component holoenzyme by recruiting one of several adaptors with BTB/POZ domain, such as SPOP and Keap1 to confer substrate specificity (Genschik et al., 2013). Notably, we found that Nanog specifically interacted with SPOP, but not other Cullin 3-based E3 ligase adaptor proteins including Keap1, KLHL2, KLHL3, KLHL12, KLHL20, or COP1/ DET1, a Cullin 4-based E3 ligase substrate adaptor protein (Lau and Deng, 2012; Marine, 2012) (Figures 1C and S1F). Importantly, we also found that Nanog failed to interact with Fbxw8, the only characterized Cullin 7-interacting substrate adaptor protein (Ponyeam and Hagen, 2012; Sarikas et al., 2008), in cells (Figure S1G), further suggesting that Cullin 3, but not Cullin 7, is likely to play a critical role in regulating Nanog stability.

Moreover, SPOP specifically interacted with Nanog both *in vitro* and in cells (Figures 1D–1F) but not with other stem cell determining factors such as Oct4, Sox2, and Klf4 in cells (Figure 1D). In further support of SPOP as an adaptor protein for the interaction between Cullin 3 and Nanog, we found that depletion of *SPOP* largely disrupted Cullin 3 interaction with Nanog in both PC3 and C4–2 cell lines (Figures S1H and S1I). Notably, ectopic expression of SPOP could markedly decrease the abundance of Nanog (Figure 1G), but not other stem-cell-determining factors (Figure S1J), largely through shortening the half-life of Nanog in cells (Figures S1K and S1L). Furthermore, SPOP-dependent degradation of Naong could be blocked by the proteasome inhibitor, MG132 (Figure 1H). Consistently, SPOP, but neither Keap1 nor COP1/DET1, could promote the poly-ubiquitination and subsequent degradation of Nanog in cells (Figures 1I and 1J). These results advocate the Cullin 3^{SPOP} E3 ubiquitin ligase complex as a novel upstream negative regulator for Nanog stability through promoting its poly-ubiquitination.

As Nanog plays an oncogenic role in multiple types of human malignancies including PrCa, contributing to tumorigenesis in part through initiating and preserving cancer stem cells (Wong and Cheung, 2016; Iv Santaliz-Ruiz et al., 2014; Wang et al., 2013a), we

hypothesized that SPOP might control CSC traits via governing the destruction of Nanog. In support of this model, we found that SPOP dramatically suppressed Nanog-mediated prostate cancer stem cell traits including sphere formation, self-renewal ability, as well as the $Aldh^+$ prostate cancer cell populations (Figures 1K–1M, S1M, and S1N). Moreover, ectopic expression of SPOP also dramatically inhibited the ability of Nanog in promoting *in vitro* cellular transformation properties of PrCa cells including anchorage-independent growth (Figure S1O) and colony formation (Figure S1P).

More importantly, to isolate cancer stem cell subpopulation from human prostate cancer cells, we explored sorting prostate cancer stem cells by fluorescence-activated cell sorting (FACS) analysis using most of reported stem cell surface markers, including CD44 (Patrawala et al., 2006; Collins et al., 2005), CD133 (Collins et al., 2005; Richardson et al., 2004), Trop2 (Goldstein et al., 2010; Goldstein et al., 2008), CD117 (Leong et al., 2008), CD24 (Hurt et al., 2008), and CD26 (Park et al., 2016; Pang et al., 2010) in various human prostate cancer cell lines (Figure S1Q). Although expression of these stem cell markers we examined varied dramatically among different prostate cancer cell lines, we found that Trop2-and CD26-positive cells exhibited reasonable population in all prostate cancer cell lines we examined (Figure S1Q). Hence, in the reminder of this study, we chose Trop2 and CD26 as stem cell markers to sort the AR^- PC3 and AR^+ 22Rv1 cells in our experimental conditions.

Notably, we found that the Nanog expression was relatively higher in Trop2/CD26 double positive ($Trop2^+CD26^+$) cells than Trop2/CD26 double negative ($Trop2^-CD26^-$) cells in both PC3 and 22Rv1 cell lines (Figure S1R). Moreover, we also observed SPOP expression exhibited an inverse correlation with Nanog expression between $Trop2^+CD26^+$ and $Trop2^-CD26^-$ cells (Figure S1R). Consistently, downstream target genes of Nanog including Sox2, Oct4, Klf4, Bmi1, Snai1, and Ccnd1 were upregulated in $Trop2^+CD26^+$ cells compared with $Trop2^-CD26^-$ cells, which suggested that endogenous Nanog is activated in $Trop2^+CD26^+$ cells (Figures S1S and S1T). Furthermore, compared to $Trop2^-CD26^-$ cells, $Trop2^+CD26^+$ cells exhibited higher capability for sphere formation and self-renewal in both AR^- PC3 and AR^+ 22Rv1 cell lines (Figures 1N–1Q). More importantly, knockdown of endogenous *Nanog* in FACS-sorted $Trop2^+CD26^+$ cells dramatically reduced prostate cancer stem cell traits including the ability of sphere formation and the population of $Aldh^+$ cells, indicating that the prostate cancer stem cell properties of $Trop2^+CD26^+$ cells depend on endogenous Nanog expression (Figures S1U–S1X). To further confirm whether $Trop2^+CD26^+$ cell population possesses higher tumorigenic ability *in vivo*, we serially diluted $Trop2^+CD26^+$ and $Trop2^-CD26^-$ PC3 cells (10^5, 10^4, 10^3, and 10^2) and subcutaneously injected these cells into nude mice. We found that $Trop2^+CD26^+$ PC3 cells exhibit significantly higher tumor incidence than $Trop2^-CD26^-$ cells (Figure 1R). Taken together, these results support the notion that the population of $Trop2^+CD26^+$ prostate cancer cells with higher Nanog and concomitantly lower SPOP expression possesses higher tumorigenic ability.

Depletion of *SPOP* Stabilizes Nanog, Leading to Elevated Prostate Cancer Stem Cell Properties

Consistent with a crucial role for SPOP in negatively regulating Naong stability, we found that the Nanog protein level was elevated in $Spop^{-/-}$ MEFs compared to $Spop^{+/+}$ MEFs (Figure 2A). Moreover, depletion of endogenous *SPOP* using several independent short hairpin RNAs (shRNAs) also resulted in a marked upregulation of Nanog protein abundance in various PrCa cell lines such as PC3 (Figure 2B) and DU145 cells (Figure 2C). Consistently, compared with the control, the half-life of endogenous Nanog was prolonged in shSPOP-treated cells (Figures 2D and 2E). In further support of the model that SPOP suppresses Nanog protein abundance in a poly-ubiquitination and degradation dependent manner, we found that the poly-ubiquitination of Nanog was markedly decreased upon depleting *SPOP* in cells (Figures 2F and S2A).

As the crucial role of Nanog in stemness maintenance of embryonic stem cell and cancer stem cell has been well established and extensively studied by other groups (Song et al., 2017; Jin et al., 2016; Noh et al., 2012; Chambers et al., 2003; Mitsui et al., 2003), we intend to further pinpoint whether *SPOP* deficiency upregulates prostate CSC properties in a Nanog-dependent manner. To this end, we examined the effects of *SPOP* deficiency in the presence or absence of *Nanog* on various prostate CSC traits. Notably, we found that depletion of *SPOP* in AR^- PC3 or AR^+ 22Rv1 and C4–2 cells enhanced their abilities to form spheres and self-renew (Figures 2G, 2H, and S2B–S2I), indicating SPOP as a negative regulator of prostate CSC traits. In further support of this notion, depleting *SPOP* in PC3 cells also led to elevated $Aldh^+$ cell populations (Figure 2I) as well as acquired *in vitro* cellular transformation properties including an increase in anchorage independent soft-agar growth (Figures S2J–S2L) and colony formation (Figures S2M–S2O) *in vitro*. Furthermore, we found that depletion of *SPOP* in PC3 could promote *in vivo* tumorigenesis in a xenograft mouse model (Figures 2J–2L) largely in a Nanog-dependent manner, as additional depletion of *Nanog* largely reversed the elevation of CSC traits and tumor growth in *SPOP*-depleted cells (Figures 2G–2L and S2B–S2O). RT-PCR analysis of Nanog downstream target genes including Sox2, Oct4, Klf4, Bmi1, Snail, and Ccnd1 showed that depletion of *SPOP* elevates Nanog downstream target genes transcription, which suggests that SPOP regulates endogenous Nanog transcriptional activity (Figures S2P and S2Q). These results together demonstrated that *SPOP* deficiency enhances the prostate CSC properties primarily through stabilizing the Nanog to activate its various downstream target genes.

Moreover, in keeping with a pivotal role for SPOP in suppressing cell stemness, we found that in the absence of leukaemia inhibitory factor (LIF) that functionally maintains the pluripotential state of embryonic stem cell (Smith et al., 1988), small interfering RNA (siRNA)-mediated depletion of endogenous *SPOP* resulted in a significant elevation in the undifferentiated state of mES cells (Figures 2M, 2N, and S2R). More importantly, additional depletion of endogenous *Nanog* significantly reduced siSPOP-mediated elevation in undifferentiated mES cell population (Figures 2M, 2N, and S2R). Together, these results suggest that SPOP is a suppressor of stem cell maintenance and *SPOP* deficiency leads to an elevation of undifferentiated mES cell population largely through upregulation of Nanog. As such, in the PrCa setting, deficiencies in the *SPOP* tumor suppressor may promote prostate

CSC traits as it does to mES cells, largely through reducing the poly-ubiquitination and subsequent degradation of the pluripotency determining factor Nanog.

PrCa-Derived *SPOP* Mutants Fail to Interact with Nanog to Promote Nanog Poly-ubiquitination and Subsequent Degradation

Recent large-scale sequencing studies showed that *SPOP* is one of the most frequently mutated genes in human PrCa (Cancer Genome Atlas Research Network, 2015). Electronic address and Barbieri et al., 2012; Berger et al., 2011. Structurally, SPOP comprises an N-terminal substrate-interacting MATH domain and a C-terminal Cullin 3-interacting BTB domain (Figure 3A). Notably, we observed that deletion of the MATH domain could disrupt SPOP interaction with Nanog and abrogate SPOP-mediated Nanog destruction (Figures 3B and 3C). Consistently, compared with WT SPOP (SPOP-WT), loss of either the MATH domain or BTB domain mutant abolished the ability of SPOP to shorten the half-life of Nanog, largely due to their deficiency in earmarking Nanog for poly-ubiquitination in cells (Figures S3A–S3C).

To date, most of the identified *SPOP* somatic mutations in PrCa including Y87C, F102C, and W131G are clustered in the MATH domain, which presumably impairs their interaction with the substrate (Geng et al., 2013; Zhuang et al., 2009). Consistently, these prostate-cancer-derived SPOP mutants indeed failed to interact with Nanog both in cells and *in vitro* (Figures 3D and 3E), thereby being incapable of promoting Nanog for poly-ubiquitination (Figure 3F) and subsequent degradation in cells (Figure 3G). In keeping with these findings, ectopic expression of SPOP-WT, but not PrCa-derived SPOP mutants, dramatically shortened the half-life of Nanog in cells (Figures S3D and S3E).

Next, to examine whether prostate-cancer-patient-derived SPOP mutants affect prostate CSC properties, we ectopically introduced SPOP-WT, the Y87C, F102C, W131G mutants, as well as the empty vector (EV) in PC3 cells. In line with our model that PrCa-derived mutations impair SPOP-mediated degradation of Nanog, we found that SPOP-WT, but not SPOP mutants including Y87C, F102C, and W131G, in PC3 cells decreased the abundance of endogenous Nanog (Figure S3F). Moreover, SPOP-WT, but not prostate-cancer-patient-derived SPOP mutants, was capable of suppressing CSC traits of PC3 cells including reducing sphere formation in cells (Figure 3H), self-renewal (Figure 3I), as well as the populations of $Aldh^+$ cells (Figure 3J). These results demonstrated that SPOP-WT, but not PrCa-derived mutants, negatively regulates Nanog protein stability through promoting its poly-ubiquitination and subsequent destruction to suppress PrCa CSC traits.

Furthermore, we analyzed Nanog protein abundance in 96 human primary prostate tumor specimens. First, we identified 12 *SPOP*-mutation and 84 *SPOP*-WT cases through large-scale sequencing including whole-genome sequencing and RNA sequencing (RNA-seq) (An et al., 2015; Xu et al., 2012). Next, we performed immunohistochemical (IHC) staining of Nanog in two cohorts of prostate tumor specimens (Figure 3K). Nanog staining was scored as negative (0), weak (1), intermediate (2), or strong (3). Notably, IHC results showed that approximately 60% of *SPOP*-mutated tumors exhibited intermediate or strong straining of Nanog protein (Figure 3L). However, only 20% of SPOP-WT tumors exhibited intermediate or strong straining of Nanog protein, but 80% of SPOP-WT cases exhibited weak or no

staining of Nanog (Figures 3K and 3L). These results support the model that *SPOP*-deficiency positively correlates with elevation in Nanog oncoprotein abundance in a PrCa setting.

Through bioinformatic analysis of the gene signature of *SPOP* mutation versus Nanog higher expression in prostate clinical samples from The Cancer Genome Atlas (TCGA) database, we found a significant positive correlation between the expression profiles with *SPOP* mutations and Nanog higher expression in PrCa (Rho = 0.80; p < 2.2e—16) through using two-class paired significance analysis of microarray data (Figure S3G). Furthermore, compared with normal samples, there are 3,226 and 3,418 genes showing significant differential expression in *SPOP* mutation and Nanog higher expression prostate tumor samples, respectively (Figure S3H). Moreover, there are 1,255 genes that are co-regulated by *SPOP* mutation and Nanog higher expression events (Figures S3H and S3I). Taken together, these results indicate that *SPOP* mutation and Nanog higher expression might share common gene signatures in PrCa pathophysiological conditions. Therefore, SPOP mutations with elevated expression of Nanog protein and its downstream targets may favor prostate CSC traits.

SPOP Promotes the Poly-ubiquitination and Subsequent Degradation of Nanog in a Degron-Dependent Manner

A PEST motif sequence (rich in proline, glutamine, serine, and threonine) from amino acid 47 to 72 located in the N terminus of Nanog has been reported to play a critical role for Nanog poly-ubiquitination in cells (Ramakrishna et al., 2011). However, the specific E3 ligase capable of recognizing this degron motif to earmark Nanog for poly-ubiquitination-mediated destruction remains largely unknown. Through examination of Nanog protein sequence, we identified an evolutionarily conserved putative SPOP recognizable degron, ^{66}PDSST^{70}, in the PEST motif sequence, which fits the canonical SPOP degron consensus motif F-P-S-S/T-S/T (F-nonpolar; P, polar) (Zhuang et al., 2009) (Figure 4A). Importantly, deleting the putative motif 66PDSST^{70} (ΔPDSST) impaired the interaction between Nanog and SPOP both in cells and *in vitro* (Figures 4B, 4C, and S4A), leading to acquired resistance to SPOP-mediated destruction (Figures 4D–4F) and poly-ubiquitination in cells and *in vitro* (Figures 4G and S4B).

Furthermore, we found that ectopic expression of Naong-WT and, to a much greater extent, Nanog-ΔPDSST in part due to elevated stability (Figures S4C and S4D), led to an elevation of various CSC traits in PC3 cells including sphere formation ability *in vitro* (Figure S4E), self-renewal (Figure S4F), and Aldh$^+$ cell populations (Figure S4G) to favor *in vitro* cellular transformation properties such as anchorage-independent growth (Figure S4H) and colony formation (Figure S4I) *in vitro*. More importantly, introducing SPOP could efficiently suppress the ability of Nanog-WT, but not the degron-deficient Nanog-ΔPDSST mutant, in elevating PrCa CSC traits including sphere formation ability *in vitro* (Figures 4H, S4J, and S4K) and Aldh$^+$ cell populations (Figure 4I) to favor *in vivo* tumorigenesis in a xenograft model (Figures 4J, 4K, and S4L).

In keeping with the results that depletion of *SPOP* upregulates the colony number of alkaline-phosphatase-stainingpositive (AP$^+$) mES in the absence of LIF (Figures 2M and

2N), we found that ectopic expression of SPOP could significantly suppress Nanog WT-mediated AP^+ colony number of mES in the absence of LIF (Figures 4L and S4M). However, SPOP did not inhibit the colony number of degron-deficient Nanog mutant-mediated AP^+ cell population of mES (Figures 4L and S4M). Taken together, these results demonstrate that the ^{66}PDSST^{70} degron motif within the N-terminal PEST sequence of Nanog is required for SPOP to control Nanog destruction, thereby governing prostate CSC traits and subsequent tumorigenesis.

Cancer-Patient-Derived Nanog Mutation (S68Y) in the Degron Motif Confers Resistance to SPOP-Mediated Destruction of Nanog

Given that SPOP promotes the poly-ubiquitination and degradation of Nanog in a degron motif dependent manner (Figure 4), we would like to further explore whether in human cancers, besides mutating the E3 ligase, SPOP, there are other layers of mutations such as at the substrate level, allowing Nanog to evade SPOP-mediated destruction. To this end, we examined TCGA database (cBioPortal) and found one somatic mutation (S68Y) in the SPOP-binding consensus motif (Figure 5A). Importantly, both in cells and *in vitro* binding assays demonstrated that the S68Y-Nanog mutant is largely deficient in binding with SPOP (Figures 5B and 5C). In further support of SPOP as an adaptor protein for the interaction between Nanog and Cullin 3, we found that the S68Y-Nanog mutant that is deficient in binding with SPOP (Figures 5B and 5C) also lost its binding with Cullin 3 in cells (Figure S5A). As a result, unlike WT-Nanog, the Nanog-S68Y mutant was resistant to SPOP-mediated poly-ubiquitination and degradation events (Figures 5D and 5E). Accordingly, the Nanog-S68Y mutant displayed a prolonged half-life compared to its WT counterpart in cells (Figures 5F and 5G).

To gain further insight into whether by evading the SPOP-mediated degradation, Nanog-S68Y enhances its oncogenic roles in cells, we generated PC3 stable cell lines ectopically expressing Nanog-WT, Nanog-S68Y, as well as EV as a negative control. Consistently, we found that the Nanog-S68Y mutant was more stable than Nanog-WT in PC3 cells (Figures S5B and S5C). More importantly, ectopic expression of Naong-WT, and to a much greater extent, Nanog-S68Y, caused an elevation of CSC traits including sphere formation ability (Figure S5D), selfrenewal (Figure S5E), and $Aldh^+$ cell populations (Figure S5F) to acquire cellular transformation properties such as anchorage-independent growth (Figure S5G) and colony formation (Figure S5H) *in vitro*. Notably, introducing SPOP in Nanog-expressing PC3 cells could dramatically suppress Nanog-WT, but not S68Y-mediated enhancement in CSC traits including sphere formation ability (Figures 5H and 5I) and $Aldh^+$ cell populations (Figure 5J), which correlates with the ability of SPOP in reducing the protein abundance of Nanog-WT, but not Nanog-S68Y in these cells (Figure S5I). Hence, these results together suggest that cancer-patient-derived mutant S68Y is more oncogenic than Nanog-WT in conferring CSC traits or cellular transformation properties, largely due to its acquired ability to evade SPOP-mediated poly-ubiquitination and degradation process to favor prostate tumorigenesis.

Pin1 Inhibitors Promote SPOP-Mediated Destruction of Nanog to Suppress Prostate CSC Traits

It has been previously reported that the prolyl-isomerase Pin1 could stabilize Nanog through recognizing the pSer/pThr-Pro motifs in Nanog and subsequently inhibit its poly-ubiquitination and degradation through an unidentified E3 ubiquitin ligase (Moretto-Zita et al., 2010). Given that our results pinpoint SPOP as the upstream physiological E3 ligase responsible for Nanog poly-ubiquitination and degradation in the PrCa setting, we intended to further explore whether the Pin1 oncoprotein stabilizes the Nanog oncoprotein through disrupting the SPOP/ Nanog destruction pathway. In keeping with this notion, we found that Pin1 WT (Pin1-WT), but not its enzymatically inactive mutant W34A/K63A (Tun-Kyi et al., 2011), suppressed SPOP-mediated degradation of Nanog largely through disrupting the interaction between SPOP and Nanog in cells (Figures 6A and 6B). In keeping with these results, Pin1-WT, but not the W34A/K63A mutant, could dramatically extend the half-life of Nanog through inhibiting SPOP-mediated Nanog poly-ubiquitination in cells (Figures 6C–6E and S6A).

Given that Pin1 recognizes the pSer/pThr-Pro motif and two SP sites (S65 and S71) located nearby the SPOP binding motif on the Nanog protein (Figure 6F), we speculated that Pin1 might disrupt Nanog interaction with SPOP through binding these two SP sites. In keeping with this notion, compared to Nanog WT, the Nanog S65A/S71A mutant dramatically decreased its ability to associate with Pin1 (Figure 6G), while exhibiting an elevated interaction with SPOP in cells (Figure 6H). Notably, compared with *Pin1*$^{+/+}$ MEFs, the abundance of endogenous Nanog protein was markedly reduced in *Pin1*$^{-/-}$ MEFs with no significant change of SPOP protein abundance (Figure 6I). Furthermore, unlike Nanog, depletion of *Pin1* in MEFs did not lead to any detectable change in protein abundance of other well-characterized SPOP substrates including TRIM24 and DEK (Figure 6I), arguing that instead of modulating SPOP protein abundance or E3 ligase activity *per se*, Pin1 mainly regulates the protein stability of Nanog, but not other SPOP substrates, presumably by competing for binding sites on the Nanog protein with SPOP, thereby interfering SPOP-mediated Nanog degradation.

Pin1 has been identified as an attractive drug target for cancer therapies (Zhou and Lu, 2016; Theuerkorn et al., 2011), and several Pin1 inhibitors have been developed for potential anticancer agents (Wei et al., 2015; Uchida et al., 2003; Hennig et al., 1998). Notably, we found that well-characterized Pin1 inhibitors, PiB (Rustighi et al., 2014; Moretto-Zita et al., 2010; Uchida et al., 2003) and Juglone (Hennig et al., 1998), could promote SPOP-mediated Nanog degradation (Figures 6J and S6B) through elevating Nanog interaction with SPOP in cells (Figures 6K and S6C). Given that Juglone was the first identified Pin1 inhibitor while PiB was recently demonstrated to be a relatively more specific Pin1 inhibitor (Uchida et al., 2003), in the reminder of this study, we primarily used PiB to pharmacologically inhibit Pin1 enzymatic activity in cells.

In keeping with the model that Pin1 largely stabilize Nanog by impairing its recognition by SPOP, PiB could dramatically decrease Nanog protein levels in shScr-treated PC3 cells, but not in shSPOP-treated cells (Figure 6L). Consistently, PiB could markedly suppress CSC traits including sphere formation ability (Figures 6M and 6N) and Aldh^{+} cell populations

(Figure 6O) in shScr-control, but not in *SPOP*-depleted PC3 cells (Figures 6M and 6O). Furthermore, the Pin1 inhibitor, PiB, could suppress the sphere formation ability of PC3 cells ectopically expressing SPOP WT but not cancer-derived F102C and W131G mutants (Figures 6P and 6Q), both of which were deficient in binding with Nanog (Figures 3D and 3E).

In further support of the notion that Pin1 largely regulates Nanog protein stability in a SPOP-dependent manner, we found that although PiB treatment led to a marked decrease in protein abundance of Naong WT, PiB was incapable of further inducing the degradation of cancer-derived S68Y mutant (Figure S6D), which was also deficient in binding with SPOP (Figure 5B). In keeping with these findings, Pin1 inhibitors including PiB and Juglone dramatically inhibited the ability of Nanog-WT, but not the SPOP non-interacting mutant S68Y-Nanog, to confer CSC traits including $Aldh^+$ cell populations in PC3 cells (Figures S6E and S6F) or gain cellular transformation properties including anchorage-independent growth (Figures S6G and S6H) and colony formation (Figures S6I and S6J). Taken together, these results coherently demonstrate that pharmacological inhibition of the Pin1 oncoprotein can promote SPOP-mediated degradation of Nanog to suppress prostate CSC traits in WT, but not *SPOP*-deficient PrCa cells.

DISCUSSION

Previous studies showed that SPOP has context-dependent roles in governing tumorigenesis, exerting its oncogenic or tumor suppressive function depending on the specific tumor types or cellular contexts (An et al., 2015; An et al., 2014; Geng et al., 2014; Li et al., 2014; Theurillat et al., 2014). Although increasing evidence demonstrates that SPOP may function as a tumor suppressor in the PrCa setting, the precise molecular mechanism(s) remains poorly defined. Here, we provide experimental evidence demonstrating that SPOP functions largely as a tumor suppressor in PrCa through targeting the pluripotency-maintaining transcription factor, Nanog, for poly-ubiquitination and subsequent degradation to inhibit prostate CSC traits. More importantly, prostate cancer-derived SPOP mutants clustered in its substrate-recruiting MATH domain disrupted the ability of SPOP in binding and promoting Nanog poly-ubiquitination and destruction, as well as suppressing prostate CSCs characteristics (Figure 3). These results therefore suggest that SPOP mutations may favor tumorigenesis in part through elevating the pluripotency-determining factor, Nanog, to confer CSC traits, at least in the prostate cancer setting.

Currently, it is well accepted that prostate basal cells and luminal cells in adults are independently sustained and can both serve as a cellular origin or stem cell pool of prostate cancer (Wang et al., 2013b; Choi et al., 2012; Goldstein et al., 2010; Wang et al., 2009). Recently, several reports showed that SPOP mutations exist in both human primary prostate tumor and metastatic prostate tumor (Cancer Genome Atlas Research Network, 2015; Baca et al., 2013; Barbieri et al., 2012). Moreover, SPOP mutation is found to be an early event in the natural history of PrCa, while PTEN and TP53 lesions mainly occur in relatively later stages (Barbieri et al., 2014; Baca et al., 2013). Interestingly, SPOP mutations and PTEN abnormalities rarely occur together in clinically localized disease, but these mutations begin to overlap and co-occur with advanced PrCa disease (Barbieri et al., 2014; Barbieri et al.,

2012; Grasso et al., 2012). Taken together, these studies indicate that SPOP mutation might be concentrated in prostate tumor-initiating cells or prostate CSCs to govern prostate tumorigenesis. However, it will be important to further validate whether these SPOP mutations enriched in prostate CSCs in the future.

Furthermore, the cancer patient-derived Nanog mutant S68Y, which locates in the SPOP-binding consensus motif ^{66}PDSST^{70}, was also deficient in binding with SPOP. As a result, the S68Y-Nanog mutant evaded SPOP-mediated degradation, thereby becoming more oncogenic than SPOP-WT to favor tumorigenesis in part by conferring prostate CSC traits (Figure 5). More interestingly, although previous reports showed that the oncogenic isomerase, Pin1, could control ESCs self-renewal through inhibiting the poly-ubiquitination and degradation of Nanog (Moretto-Zita et al., 2010), the physiological upstream E3 ligase for Nanog is largely unknown to date. Here, our results identified Cullin 3^{SPOP} as the physiological E3 ubiquitin ligase complex responsible for Nanog poly-ubiquitination and degradation. More importantly, we identified the Pin1 oncoprotein as the upstream regulator of Nanog stability in a SPOP-dependent manner, which protects Nanog from SPOP-mediated poly-ubiquitination and degradation events to favor PrCa tumorigenesis (Figure 6). Accordingly, Pin1 inhibitors can inhibit Nanog-mediated prostate CSC traits largely by promoting the SPOP-mediated degradation of Nanog.

These results therefore suggest that aberrant stabilization of the Nanog oncoprotein in PrCa through various means, either by mutating the upstream SPOP E3 ligase, by genetic mutations to inactivate the degron motif in Nanog, or by overexpression of the Pin1 oncoprotein, may lead to aberrant activation of a cohort of pluripotency related Naong downstream target genes to favor tumorigenesis in part through promoting CSC traits (Figure S6K). To this end, our results suggest in clinical settings, developing novel therapeutic strategies such as the Pin1 inhibitor that aims to reduce Nanog abundance based on the genetic status of *SPOP* and/or *Nanog* mutation could better design precision medicine regimens for the treatment of PrCa patients.

STAR*METHODS

Detailed methods are provided in the online version of this paper and include the following:

KEY RESOURCES TABLE

REAGENT or RESOURCE	SOURCE	IDENTIFIER
Antibodies		
Anti-SPOP	Proteintech	Cat # 16750–1-AP; RRID: AB_2756394
Anti-Nanog	EMD Millipore	Cat # AB5731; RRID: AB_2267042
Anti-Nanog	Cell Signaling Technology	Cat # 4903; RRID: AB_10559205
Anti-Cullin 3	Cell Signaling Technology	Cat # 2759; RRID: AB_2086432
Anti-GST	Cell Signaling Technology	Cat # 2625; RRID: AB_490796
Anti-Myc tag antibody	Cell Signaling Technology	Cat # 2278; RRID: AB_490778

REAGENT or RESOURCE	SOURCE	IDENTIFIER
Anti-Myc tag antibody	Cell Signaling Technology	Cat # 2276; RRID: AB_331783
Anti-HA tag antibody	Santa Cruz	Cat # SC-805; RRID: AB_631618
Anti-p27	Santa Cruz	Cat # SC-527; RRID: AB_632131
Anti-Cyclin A	Santa Cruz	Cat # SC-751; RRID: AB_631329
Anti-Cyclin E	Santa Cruz	Cat # SC-247; RRID: AB_627357
Anti-Vinculin	Sigma	Cat # V4505; RRID: AB_477617
Anti-Tubulin	Sigma	Cat # T5168; RRID: AB_477579
Anti-Flag	Sigma	Cat #F7425; RRID: AB_439687
Anti-Flag	Sigma	Cat # F3165; RRID: AB_259529
Anti-HA Agarose	Sigma	Cat # A2095; RRID: AB_257974
Anti-Flag M2 affinity gel	Sigma	Cat # A2220; RRID: AB_10063035
Anti-Purified anti-HA.11 Epitope Tag Antibody	BioLegend	Cat # MMS-101P; RRID: AB_10064068
Anti-GFP	Clontech	Cat #632375; RRID: AB_2756343
Peroxidase-conjugated anti-mouse secondary antibody	Sigma-Aldrich	Cat # A-4416; RRID: AB_258167
Peroxidase-conjugated anti-rabbit secondary antibody	Sigma-Aldrich	Cat # A-4914; RRID: AB_258207
Anti-human Trop2 (EGP-1) PE	eBioscience	Cat #12–6024-42; RRID: AB_2572648
Anti-human/mouse CD49f APC (eBioGoH3)	eBioscience	Cat #17–0495-82; RRID: AB_2016694
Anti-hCD133 Alexa Fluro 488 conjugated	R&D systems	Cat # FAB11331G; RRID: AB_2756395
Anti-human CD117 (c-kit) PE (104D2)	Biolegend	Cat # 313204; RRID: AB_314983
Anti-human/mouse CD24 APC	eBioscience	Cat # 17–0247-41; RRID: AB_10718529
Anti-human CD26 PE	eBioscience	Cat # 12–0269-41; RRID: AB_2572554
Anti-human CD26 APC	Invitrogen	Cat # CD2605; RRID: AB_1468826
Mouse IgG2A Alexa Fluor 488-conjugated antibody	R&D systems	Cat # IC003G; RRID: AB_10718683
Mouse IgG2A Kappa isotype control, PE	eBioscience	Cat # 12–4724-41; RRID: AB_1603328
Mouse IgG2A Kappa isotype control, APC	eBioscience	Cat # 17–4724-41; RRID: AB_10598641
Bacterial and Virus Strains		
XL10 Gold *Escherichia coli*	Agilent	Cat # 200314
BL21(DE3) *Escherichia coli*	Dr. William G. Kaelin, Jr., Dana-Farber Cancer Institute	N/A
Chemicals, Peptides and Recombinant Proteins		
Juglone	Sigma-Aldrich	Cat # 420120–250MG
PiB	Sigma-Aldrich	Cat # B7688
MG132	Enzo life science	Cat # BML-PI102–0005
MLN4924	Medchemexpress LLC	Cat # HY-70062

REAGENT or RESOURCE	SOURCE	IDENTIFIER
GST protein	In our lab	N/A
GST-Nanog WT	In our lab	N/A
GST-Nanog ΔPDSST	In our lab	N/A
His-SPOP	In our lab	N/A
Critical Commercial Assays		
QuickChange XL Site-Directed Mutagenesis Kit	Stratagene	Cat # 200516
The ALDEFLUOR™ Assay kit	StemCell Technologies	Cat # 01700
Experimental Models: Cell Lines		
HEK293T	Dr. William G. Kaelin, Jr., Dana-Farber Cancer Institute	N/A
PC3	In our lab	N/A
DU145	In our lab	N/A
22Rv1	In our lab	N/A
C4–2	In our lab	N/A
MEFs *SPOP*$^{+/+}$ and *SPOP*$^{-/}$	Dr. Nicholas Mitsiadesa, Baylor College of Medicine	N/A
MEFs *Pin*$^{+/+}$ and *Pin1*$^{-/-}$	Dr. Kun Ping Lu, Beth Israel Deaconess Medical Center	N/A
Experimental Models: Organisms/Strains		
Nude mice: NCRNU-F: CrTac:NCr-*Foxn1*^{nu}	Taconic Biosciences	Cat # NCRNU-F
Recombinant DNA		
pcDNA3-HA-Nanog WT	In this paper	N/A
pcDNA3-HA-Nanog ΔPDSST	In this paper	N/A
pcDNA3-HA-Nanog S68Y	In this paper	N/A
pGEX-4T-1-Nanog WT	In this paper	N/A
pGEX-4T-1-Nanog ΔPDSST	In this paper	N/A
pLenti-Flag-Nanog	In this paper	N/A
pCMV-Flag-SPOP	(Gan et al., 2015)	N/A
pCMV-Flag-SPOP Y87C	(Gan et al., 2015)	N/A
pCMV-Flag-SPOP F102C	(Gan et al., 2015)	N/A
pCMV-Flag-SPOP W131G	(Gan et al., 2015)	N/A
Myc-Cullin 1–5	(Gan et al., 2015)	N/A
Flag-Keap1	(Gan et al., 2015)	N/A
Flag-COP1	(Gan et al., 2015)	N/A
Flag-DET1	(Gan et al., 2015)	N/A
pGEX-4T-1-SPOP	(Gan et al., 2015)	N/A
pLKO-shCullin 3	(Gan et al., 2015)	N/A
Flag-Oct4	In this paper	N/A

REAGENT or RESOURCE	SOURCE	IDENTIFIER
Flag-Sox2	In this paper	N/A
Flag-Klf4	In this paper	N/A
pLKO-shSPOP	(Gan et al., 2015)	N/A
pCMV-Flag-SPOP ΔMATH	(Gan et al., 2015)	N/A
pCMV-Flag-SPOP ΔBTB	(Gan et al., 2015)	N/A
HA-Pin1 WT	Dr. Kun Ping Lu, Beth Israel Deaconess Medical Center	N/A
HA-Pin1 W34A/K63A	Dr. Kun Ping Lu, Beth Israel Deaconess Medical Center	N/A
Oligonucleotides		
Quantitative RT-PCR primers (Refer to Table S1)	In this paper	N/A
Deposited Data		
Original blots for Figures 1, 2, 3, 4, 5, 6, and S1–S6.	https://data.mendeley.com/datasets/tpz7kh7pdv/1	Mendeley Dataset

CONTACT FOR REAGENT AND RESOURCE SHARING

Further information and requests for reagents may be directed to and will be fulfilled by the Lead Contact, Wenyi Wei (wwei2@bidmc.harvard.edu).

EXPERIMENTAL MODEL AND SUBJECT DETAILS

Cell Culture—All human prostate tumor cell lines (male) including PC3, DU145, 22Rv1 and C4–2 cells were maintained in RPMI 1640 medium supplemented with 10% FBS, 100 units of *penicillin* and 100 mg/ml streptomycin in a sterile 37°C incubator with a humidified 5% CO2 atmosphere. HEK293T and mouse embryonic fibroblasts (MEFs) $Spop^{+/+}$ and $Spop^{-/-}$cells (a kind gift of Dr. Nicholas Mitsiadesa, Baylor College of Medicine, Houston, TX) were cultured in Dulbecco's modified Eagle's medium (DMEM) supplemented with 10% FBS, 100 units of *penicillin* and 100 mg/ml streptomycin. CJ7 mouse embryonic stem cells were cultured in Knockout™ DMEM supplemented with 15% ES grade FBS (Hyclone), 1000U/ml LIF (Millipore), 1X non-essential amino acid, 0.1 mM b-Mercaptoethanol and glutamine plus pen-strep on a MEF feeder layer.

Mouse Xenograft Assays—5×10^6 PC3 cells stably expressing indicated constructs in Figures 2J–2L, 4J, and 4K were injected into the flank of 6 (in Figures 2J–2L) or 8 (in Figures 4J and 4K) male nude mice (NCRNU-M-M from Taconic, 4–5 weeks of age). Tumor size was measured every two days with a caliper, and the tumor volume was determined with the formula: L x $W^2 \times 0.5$, where L is the longest diameter and W is the shortest diameter. 18 days after injection, mice were sacrificed and xenografted solid tumors were dissected, then tumor weights were measured and recorded post-necropsy.

***In Vivo* Serial Limiting Dilution Xenograft Assays—**PC3 cells were sorted by FACS analysis with anti-Trop2 PE and anti-CD26 APC. $Trop2^{+}CD26^{+}$ versus $Trop2^{-}CD26^{-}$PC3

cells were serially diluted (10^5, 10^4, 10^3 and 10^2) and injected into the flank of 6 male nude mice (NCRNU-M-M from Taconic, 4–5 weeks of age). Mice were monitored for tumor volumes every three days after initial treatment and mice were sacrificed when tumor volume exceeded 1500 mm^3. The frequency of cancer stem cells (CSCs) and the comparison of the difference between the two groups were calculated using ELDA (Extreme Limiting Dilution Analysis) online software (http://bioinf.wehi.edu.au/software/elda/). ***p<0.001 (*Chisq*-test).

Patient Prostate Tumor Tissues Samples and Immunohistochemical (IHC) Staining—The prostate tumor specimens (male) were obtained from Shanghai Changhai Hospital in China. Usage of these specimens was approved by the Institute Review Board of Shanghai Changhai Hospital. For IHC, the paraformaldehyde fixed paraffin embedded prostate tumor samples were deparaffinized in xylene (3X10 min), rehydrated through a series of graded alcohols (100%, 95%, 85%, and 75%) to water. Samples were then subjected to heat-mediated antigen retrieval at 95°C for 20 min. UltraSensitive ™ S-P (Rabbit) IHC Kit (KIT-9706, Fuzhou Maixin Biotech) was used by following the manufacturer's instructions with minor modification. Briefly, sections were incubated with 3% H_2O_2 for 15 minutes at room temperature to quench endogenous peroxidase activity. After incubating in normal goat serum for 1 hour, sections were incubated with the primary antibody against Nanog (dilution 1:200; Cell Signaling Technology; product Number: 4903) at 4°C overnight. The sections were then washed 3 times in PBS and treated for 30 minutes with biotinylated goat-anti-rabbit IgG secondary antibodies (Fuzhou Maixin Biotech). After washing three times in PBS, sections were incubated with streptavidin-conjugated HRP (Fuzhou Maixin Biotech). After washing three times in PBS for 5 minutes, specific detection was developed with 3,3'-diaminobenzidine (DAB-2031, Fuzhou Maixin Biotech). Images were taken by using an Olympus camera and matched software. The expression level of Nanog in prostate cancer tumor samples was determined according to the intensity of the staining as 0, negative; 1, weak expression; 2, moderate expression and 3, strong expression. The Mann-Whitney test was used to compare the difference in Nanog expression between *SPOP* mutated and wide type cases. $p < 0.05$ was considered as significant.

METHOD DETAILS

ALDH Enzymatic Activity—The ALDEFLUOR™kit was used to monitor the population with a high ALDH enzymatic activity according to the manufacturer's instructions (StemCell Technologies). Briefly, cells (1310^5 cells/ml) were suspended in ALDEFLUOR assay buffer containing ALDH substrate and incubated 30 minutes at 37°C. As negative control, an aliquot for each sample of cells was treated with the specific ALDH inhibitor diethylaminobenzaldehyde (DEAB). Following incubation, all samples were centrifuged for 5 minutes at 250 × g and the supernatant were removed. Cell pellets were resuspended in 0.5 mL of ALDEFLUOR™ Assay Buffer and were analyzed by using the flow cytometer (BD Bioscience).

Sphere-Formation Assays—5,000 cells/well were plated in 6-well ultra-low attachment plates (Corning) in serum-free prostate epithelial cell growth medium (PrEGM) (Lonza) supplemented with 1 × B27 (Invitrogen). Fresh media were added every 3 days. Floating

spheres that grew in 1–2 weeks were counted and taken pictures. Within an experiment, each condition was determined in triplicate. Results were representative of three independent experiments.

Immunoblot and Immunoprecipitation—Cells were lysed in EBC buffer (50 mM Tris pH 7.5, 120 mM NaCl, 0.5% NP40) supplemented with protease inhibitors (Complete Mini, Roche) and phosphatase inhibitors (phosphatase inhibitor cocktail set I and II, Calbiochem). The protein concentrations were measured by Beckman Coulter DU-800 spectrophotometer using the Bio-Rad protein assay reagent (Bio-Rad Laboratories, CA). For immunoprecipitation assays, 1 mg whole cell lysate protein was incubated with the appropriate antibody-conjugated beads (8 ml) or antibody (1–2 mg) for 4 hours or overnight at 4°C. The recovered immuno-complexes were washed four times with NETN buffer (20 mM Tris, pH 8.0, 100 mM NaCl, 1 mM EDTA and 0.5% NP-40) before being resolved by SDS-PAGE and immunoblotted with indicated antibodies.

***In Vivo* Ubiquitination Assays—**PC3 cells with 80% confluence were transfected with His-ubiquitin and the desired constructs. 36 hours post-transfection, cells were treated with 30 mM MG132 for 6 hours and lysed in buffer A (6 M guanidine-HCl, 0.1 M Na2HPO4/NaH2PO4, and 10 mM imidazole [pH 8.0]). After sonication, the lysates were incubated with nickel-nitrilotriacetic acid (Ni-NTA) beads (QIAGEN) for 3 hours at room temperature. Subsequently, the His pull-down products were washed twice with buffer A, twice with buffer A/TI (1 volume buffer A and 3 volumes buffer TI), and one time with buffer TI (25 mM Tris-HCl and 20 mM imidazole [pH 6.8]). The pull-down proteins were resolved by SDS-PAGE for immunoblotting.

***In Vitro* Ubiquitination Assays—**For *in vitro* Nanog ubiquitination, 0.5 mg of purified GST-Nanog WT or ΔPDSST mutant from *E. coli* bacteria was incubated with 40 ng E1 (UBE1) (E-305 Boston Biochem), 0.5 mg E2 (UbcH5a) (E2–616 Boston Biochem), 10 mg His-Ub variants (Boston Biochem), 8 mM ATP, 1× ligase reaction buffer (Fisher Scientific (Thermo Fisher Scientific) # B71), and 1× Energy regeneration system (Boston Biochem #B-10), 0.5 mg E3 complex (Cullin 3/Rbx1/SPOP) at 37°C for 1 hour in 25 ml reaction mixture.

Quantitative RT-PCR Analysis—Total RNA was extracted using the QIAGEN RNeasy mini kit, and the reverse transcription reaction was performed using the ABI Taqman Reverse Transcriptional Reagents (N808–0234). After mixing the generated cDNA templates with primers/probes and ABI Taqman Fast Universal PCR Master Mix (4352042), the real-time RT-PCR was performed with the ABI-7500 Fast Real-time PCR system. SYBR green qPCR Mastermix (600828) was purchased from Agilent Technologies Stratagene. Primers were listed in Table S1.

CJ7 mESC Culture and Alkaline Phosphatase (AP) Staining—CJ7 mouse embryonic stem cells (CJ7 mESC) were cultured in Knockout™ DMEM supplemented with 15% ES grade FBS (Hyclone), 1000U/ml LIF (Millipore), 1X non-essential amino acid, 0.1 mM b-Mercaptoethanol and glutamine plus pen-strep on a MEF feeder layer. ES cell transfections were performed using Lipofectamine 2000 or Lipofectamine RNAiMAX

reagent according to manufacturer's instruction. In brief, 2000 ES cells were transfected with 200 ng of DNA plasmids or 50 nM of siRNA in a 24-well dish. Cells were recovered into completed media after 12 h post-transfection. AP staining was used to quantify the percentage of pluripotent ES cells after 72 h post-transfection.

Fluorescence Activated Cell Sorting (FACS) of Cancer Stem Cells—Prostate cancer cells including PC3 and 22Rv1 cells were stained using various fluorophore-conjugated stem cell marker antibodies and sorted using the FACSAria cell sorter at the Joslin cytometry core.

Mouse Xenograft Assays—5×10^6 PC3 cells stably expressing indicated constructs were injected into the flank of 10 male nude mice (NCRNU-M-M from Taconic, 4–5 weeks of age). Tumor size was measured every two days with a caliper, and the tumor volume was determined with the formula: L x $W^2 \times 0.5$, where L is the longest diameter and W is the shortest diameter. 18 days after injection, mice were sacrificed and xenografted solid tumors were dissected, then tumor weights were measured and recorded post-necropsy.

Bioinformatics Analysis—Spearman correlation analysis of gene expression changes in paired normal and tumor specimens with SPOP mutant prostate tumors and Nanog high expression positive prostate tumors (Rho=0.64, $p < 2.2e\text{-}16$). Each point in the scatterplot is a gene, and the x-and y-axes are the significance analysis of microarrays D-statistic for SPOP mutant and Nanog high expression samples, respectively. The D-statistic indicates the gene's direction and magnitude of differential expression in the paired tumor versus normal sample. Values in red are significantly associated with tumor (FDR<5%) in SPOP mutation and Nanog high expression samples.

Statistical Analyses—The statistical significance between experimental groups was determined by Student's *t*-test or Mann-Whitney test. The threshold for statistical significance was set to $p < 0.05$.

Supplementary Material

Refer to Web version on PubMed Central for supplementary material.

ACKNOWLEDGMENTS

We thank Drs. Jianping Guo, Tao Zhang, and Brian North in the Wei laboratory for critical reading of the manuscript. We also thank Dr. Fen Ma from Drs. Steven P. Balk and Xin Yuan laboratories and members of the Drs. Wei and Pandolfi laboratories for useful discussion. J.Z. was supported by the NCI K99/ R00 grant 1K99CA212292–01. M.C. was supported in part by the DOD Prostate Cancer Research Program (PCRP) Postdoctoral Training Award. W.W. is an LLS scholar. This work was supported in part by the NIH grants R01CA177910 and R01GM094777 to W.W.

REFERENCES

An J, Ren S, Murphy SJ, Dalangood S, Chang C, Pang X, Cui Y, Wang L, Pan Y, Zhang X, et al. (2015). Truncated ERG oncoproteins from TMPRSS2-ERG fusions are resistant to SPOP-mediated proteasome degradation. Mol. Cell 59, 904–916. [PubMed: 26344096]

An J, Wang C, Deng Y, Yu L, and Huang H (2014). Destruction of fulllength androgen receptor by wild-type SPOP, but not prostate-cancer-associated mutants. Cell Rep 6, 657–669. [PubMed: 24508459]

Baca SC, Prandi D, Lawrence MS, Mosquera JM, Romanel A, Drier Y, Park K, Kitabayashi N, MacDonald TY, Ghandi M, et al. (2013). Punctuated evolution of prostate cancer genomes. Cell 153, 666–677. [PubMed: 23622249]

Barbieri CE, Baca SC, Lawrence MS, Demichelis F, Blattner M, Theurillat JP, White TA, Stojanov P, Van Allen E, Stransky N, et al. (2012). Exome sequencing identifies recurrent SPOP, FOXA1 and MED12 mutations in prostate cancer. Nat. Genet 44, 685–689. [PubMed: 22610119]

Barbieri CE, Demichelis F, and Rubin MA (2014). The lethal clone in prostate cancer: redefining the index. Eur. Urol 66, 395–397. [PubMed: 24411284]

Berger MF, Lawrence MS, Demichelis F, Drier Y, Cibulskis K, Sivachenko AY, Sboner A, Esgueva R, Pflueger D, Sougnez C, et al. (2011). The genomic complexity of primary human prostate cancer. Nature 470, 214–220. [PubMed: 21307934]

Beroukhim R, Mermel CH, Porter D, Wei G, Raychaudhuri S, Donovan J, Barretina J, Boehm JS, Dobson J, Urashima M, et al. (2010). The landscape of somatic copy-number alteration across human cancers. Nature 463, 899–905. [PubMed: 20164920]

Cancer Genome Atlas Research Network. (2015). The molecular taxonomy of primary prostate cancer. Cell 163, 1011–1025. [PubMed: 26544944]

Chambers I, Colby D, Robertson M, Nichols J, Lee S, Tweedie S, and Smith A (2003). Functional expression cloning of Nanog, a pluripotency sustaining factor in embryonic stem cells. Cell 113, 643–655. [PubMed: 12787505]

Choi N, Zhang B, Zhang L, Ittmann M, and Xin L (2012). Adult murine prostate basal and luminal cells are self-sustained lineages that can both serve as targets for prostate cancer initiation. Cancer Cell 21, 253–265. [PubMed: 22340597]

Collins AT, Berry PA, Hyde C, Stower MJ, and Maitland NJ (2005). Prospective identification of tumorigenic prostate cancer stem cells. Cancer Res 65, 10946–10951. [PubMed: 16322242]

Dean M, Fojo T, and Bates S (2005). Tumour stem cells and drug resistance. Nat. Rev. Cancer 5, 275–284. [PubMed: 15803154]

Ferlay J, Steliarova-Foucher E, Lortet-Tieulent J, Rosso S, Coebergh JW, Comber H, Forman D, and Bray F (2013). Cancer incidence and mortality patterns in Europe: estimates for 40 countries in 2012. Eur. J. Cancer 49, 1374–1403. [PubMed: 23485231]

Gan W, Dai X, Lunardi A, Li Z, Inuzuka H, Liu P, Varmeh S, Zhang J, Cheng L, Sun Y, et al. (2015). SPOP promotes ubiquitination and degradation of the ERG oncoprotein to suppress prostate cancer progression. Mol. Cell 59, 917–930. [PubMed: 26344095]

Geng C, He B, Xu L, Barbieri CE, Eedunuri VK, Chew SA, Zimmermann M, Bond R, Shou J, Li C, et al. (2013). Prostate cancerassociated mutations in speckle-type POZ protein (SPOP) regulate steroid receptor coactivator 3 protein turnover. Proc. Natl. Acad. Sci. USA 110, 6997–7002. [PubMed: 23559371]

Geng C, Rajapakshe K, Shah SS, Shou J, Eedunuri VK, Foley C, Fiskus W, Rajendran M, Chew SA, Zimmermann M, et al. (2014). Androgen receptor is the key transcriptional mediator of the tumor suppressor SPOP in prostate cancer. Cancer Res 74, 5631–5643. [PubMed: 25274033]

Genschik P, Sumara I, and Lechner E (2013). The emerging family of CULLIN3-RING ubiquitin ligases (CRL3s): cellular functions and disease implications. EMBO J 32, 2307–2320. [PubMed: 23912815]

Goldstein AS, Huang J, Guo C, Garraway IP, and Witte ON (2010). Identification of a cell of origin for human prostate cancer. Science 329, 568–571. [PubMed: 20671189]

Goldstein AS, Lawson DA, Cheng D, Sun W, Garraway IP, and Witte ON (2008). Trop2 identifies a subpopulation of murine and human prostate basal cells with stem cell characteristics. Proc. Natl. Acad. Sci. USA 105, 20882–20887. [PubMed: 19088204]

Grasso CS, Wu YM, Robinson DR, Cao X, Dhanasekaran SM, Khan AP, Quist MJ, Jing X, Lonigro RJ, Brenner JC, et al. (2012). The mutational landscape of lethal castration-resistant prostate cancer. Nature 487, 239–243. [PubMed: 22722839]

Hennig L, Christner C, Kipping M, Schelbert B, Ruücknagel KP, Grabley S, Kuüllertz G, and Fischer G (1998). Selective inactivation of parvulin-like peptidyl-prolyl cis/trans isomerases by juglone. Biochemistry 37, 5953–5960. [PubMed: 9558330]

Hurt EM, Kawasaki BT, Klarmann GJ, Thomas SB, and Farrar WL (2008). CD44+ CD24(−) prostate cells are early cancer progenitor/stem cells that provide a model for patients with poor prognosis. Br. J. Cancer 98, 756–765. [PubMed: 18268494]

Iv Santaliz-Ruiz LE, Xie X, Old M, Teknos TN, and Pan Q (2014). Emerging role of nanog in tumorigenesis and cancer stem cells. Int. J. Cancer 135, 2741–2748. [PubMed: 24375318]

Jin J, Liu J, Chen C, Liu Z, Jiang C, Chu H, Pan W, Wang X, Zhang L, Li B, et al. (2016). The deubiquitinase USP21 maintains the stemness of mouse embryonic stem cells via stabilization of Nanog. Nat. Commun 7, 13594. [PubMed: 27886188]

Kamp WM, Wang PY, and Hwang PM (2016). TP53 mutation, mitochondria and cancer. Curr. Opin. Genet. Dev 38, 16–22. [PubMed: 27003724]

Kim SH, Kim MO, Cho YY, Yao K, Kim DJ, Jeong CH, Yu DH, Bae KB, Cho EJ, Jung SK, et al. (2014). ERK1 phosphorylates Nanog to regulate protein stability and stem cell self-renewal. Stem Cell Res 13, 1–11. [PubMed: 24793005]

Lau OS, and Deng XW (2012). The photomorphogenic repressors COP1 and DET1: 20 years later. Trends Plant Sci 17, 584–593. [PubMed: 22705257]

Leong KG, Wang BE, Johnson L, and Gao WQ (2008). Generation of a prostate from a single adult stem cell. Nature 456, 804–808. [PubMed: 18946470]

Li G, Ci W, Karmakar S, Chen K, Dhar R, Fan Z, Guo Z, Zhang J, Ke Y, Wang L, et al. (2014). SPOP promotes tumorigenesis by acting as a key regulatory hub in kidney cancer. Cancer Cell 25, 455–468. [PubMed: 24656772]

Liu W, Chang B, Sauvageot J, Dimitrov L, Gielzak M, Li T, Yan G, Sun J, Sun J, Adams TS, et al. (2006). Comprehensive assessment of DNA copy number alterations in human prostate cancers using Affymetrix 100K SNP mapping array. Genes Chromosomes Cancer 45, 1018–1032. [PubMed: 16897747]

Mani RS (2014). The emerging role of speckle-type POZ protein (SPOP) in cancer development. Drug Discov. Today 19, 1498–1502. [PubMed: 25058385]

Marine JC (2012). Spotlight on the role of COP1 in tumorigenesis. Nat. Rev. Cancer 12, 455–464. [PubMed: 22673153]

Mitsui K, Tokuzawa Y, Itoh H, Segawa K, Murakami M, Takahashi K, Maruyama M, Maeda M, and Yamanaka S (2003). The homeoprotein Nanog is required for maintenance of pluripotency in mouse epiblast and ES cells. Cell 113, 631–642. [PubMed: 12787504]

Moretto-Zita M, Jin H, Shen Z, Zhao T, Briggs SP, and Xu Y (2010). Phosphorylation stabilizes Nanog by promoting its interaction with Pin1. Proc. Natl. Acad. Sci. USA 107, 13312–13317. [PubMed: 20622153]

Nawrocki ST, Griffin P, Kelly KR, and Carew JS (2012). MLN4924: a novel first-in-class inhibitor of NEDD8-activating enzyme for cancer therapy. Expert Opin. Invest. Drugs 21, 1563–1573.

Noh KH, Kim BW, Song KH, Cho H, Lee YH, Kim JH, Chung JY, Kim JH, Hewitt SM, Seong SY, et al. (2012). Nanog signaling in cancer promotes stem-like phenotype and immune evasion. J. Clin. Invest 122, 4077–4093. [PubMed: 23093782]

Pang R, Law WL, Chu AC, Poon JT, Lam CS, Chow AK, Ng L, Cheung LW, Lan XR, Lan HY, et al. (2010). A subpopulation of CD26+ cancer stem cells with metastatic capacity in human colorectal cancer. Cell Stem Cell 6, 603–615. [PubMed: 20569697]

Park JW, Lee JK, Phillips JW, Huang P, Cheng D, Huang J, and Witte ON (2016). Prostate epithelial cell of origin determines cancer differentiation state in an organoid transformation assay. Proc. Natl. Acad. Sci. USA 113, 4482–4487. [PubMed: 27044116]

Patrawala L, Calhoun T, Schneider-Broussard R, Li H, Bhatia B, Tang S, Reilly JG, Chandra D, Zhou J, Claypool K, et al. (2006). Highly purified CD44+ prostate cancer cells from xenograft human tumors are enriched in tumorigenic and metastatic progenitor cells. Oncogene 25, 1696–1708. [PubMed: 16449977]

Ponyeam W, and Hagen T (2012). Characterization of the Cullin7 E3 ubiquitin ligase–heterodimerization of cullin substrate receptors as a novel mechanism to regulate cullin E3 ligase activity. Cell. Signal 24, 290–295. [PubMed: 21946088]

Ramakrishna S, Suresh B, Lim KH, Cha BH, Lee SH, Kim KS, and Baek KH (2011). PEST motif sequence regulating human NANOG for proteasomal degradation. Stem Cells Dev 20, 1511–1519. [PubMed: 21299413]

Richardson GD, Robson CN, Lang SH, Neal DE, Maitland NJ, and Collins AT (2004). CD133, a novel marker for human prostatic epithelial stem cells. J. Cell Sci 117, 3539–3545. [PubMed: 15226377]

Rustighi A, Zannini A, Tiberi L, Sommaggio R, Piazza S, Sorrentino G, Nuzzo S, Tuscano A, Eterno V, Benvenuti F, et al. (2014). Prolyl-isomerase Pin1 controls normal and cancer stem cells of the breast. EMBO Mol. Med 6, 99–119. [PubMed: 24357640]

Sarikas A, Xu X, Field LJ, and Pan ZQ (2008). The cullin7 E3 ubiquitin ligase: a novel player in growth control. Cell Cycle 7, 3154–3161. [PubMed: 18927510]

Siegel R, Naishadham D, and Jemal A (2013). Cancer statistics, 2013. CA Cancer J. Clin 63, 11–30. [PubMed: 23335087]

Siegel RL, Miller KD, and Jemal A (2018). Cancer statistics, 2018. CA Cancer J. Clin 68, 7–30. [PubMed: 29313949]

Siu MK, Wong ES, Kong DS, Chan HY, Jiang L, Wong OG, Lam EW, Chan KK, Ngan HY, Le XF, et al. (2013). Stem cell transcription factor NANOG controls cell migration and invasion via dysregulation of E-cadherin and FoxJ1 and contributes to adverse clinical outcome in ovarian cancers. Oncogene 32, 3500–3509. [PubMed: 22945654]

Smith AG, Heath JK, Donaldson DD, Wong GG, Moreau J, Stahl M, and Rogers D (1988). Inhibition of pluripotential embryonic stem cell differentiation by purified polypeptides. Nature 336, 688–690. [PubMed: 3143917]

Song KH, Choi CH, Lee HJ, Oh SJ, Woo SR, Hong SO, Noh KH, Cho H, Chung EJ, Kim JH, et al. (2017). HDAC1 upregulation by NANOG promotes multidrug resistance and a stem-like phenotype in immune edited tumor cells. Cancer Res 77, 5039–5053. [PubMed: 28716899]

Soucy TA, Smith PG, Milhollen MA, Berger AJ, Gavin JM, Adhikari S, Brownell JE, Burke KE, Cardin DP, Critchley S, et al. (2009). An inhibitor of NEDD8-activating enzyme as a new approach to treat cancer. Nature 458, 732–736. [PubMed: 19360080]

Stracquadanio G, Wang X, Wallace MD, Grawenda AM, Zhang P, Hewitt J, Zeron-Medina J, Castro-Giner F, Tomlinson IP, Goding CR, et al. (2016). The importance of p53 pathway genetics in inherited and somatic cancer genomes. Nat. Rev. Cancer 16, 251–265. [PubMed: 27009395]

Theuerkorn M, Fischer G, and Schiene-Fischer C (2011). Prolyl cis/trans isomerase signalling pathways in cancer. Curr. Opin. Pharmacol 11, 281–287. [PubMed: 21497135]

Theurillat JP, Udeshi ND, Errington WJ, Svinkina T, Baca SC, Pop M, Wild PJ, Blattner M, Groner AC, Rubin MA, et al. (2014). Prostate cancer. Ubiquitylome analysis identifies dysregulation of effector substrates in SPOP-mutant prostate cancer. Science 346, 85–89. [PubMed: 25278611]

Tomlins SA, Laxman B, Varambally S, Cao X, Yu J, Helgeson BE, Cao Q, Prensner JR, Rubin MA, Shah RB, et al. (2008). Role of the TMPRSS2-ERG gene fusion in prostate cancer. Neoplasia 10, 177–188. [PubMed: 18283340]

Tun-Kyi A, Finn G, Greenwood A, Nowak M, Lee TH, Asara JM, Tsokos GC, Fitzgerald K, Israel E, Li X, et al. (2011). Essential role for the prolyl isomerase Pin1 in Toll-like receptor signaling and type I interferonmediated immunity. Nat. Immunol 12, 733–741. [PubMed: 21743479]

Uchida T, Takamiya M, Takahashi M, Miyashita H, Ikeda H, Terada T, Matsuo Y, Shirouzu M, Yokoyama S, Fujimori F, et al. (2003). Pin1 and Par14 peptidyl prolyl isomerase inhibitors block cell proliferation. Chem. Biol 10, 15–24. [PubMed: 12573694]

Wang ML, Chiou SH, and Wu CW (2013a). Targeting cancer stem cells: emerging role of Nanog transcription factor. OncoTargets Ther 6, 1207–1220.

Wang X, Kruithof-de Julio M, Economides KD, Walker D, Yu H, Halili MV, Hu YP, Price SM, Abate-Shen C, and Shen MM (2009). A luminal epithelial stem cell that is a cell of origin for prostate cancer. Nature 461, 495–500. [PubMed: 19741607]

Wang Z, Inuzuka H, Fukushima H, Wan L, Gao D, Shaik S, Sarkar FH, and Wei W (2011). Emerging roles of the FBW7 tumour suppressor in stem cell differentiation. EMBO Rep 13, 36–43. [PubMed: 22157894]

Wang Z, Inuzuka H, Zhong J, Wan L, Fukushima H, Sarkar FH, and Wei W (2012b). Tumor suppressor functions of FBW7 in cancer development and progression. FEBS Lett 586, 1409–1418. [PubMed: 22673505]

Wang Z, Liu P, Inuzuka H, and Wei W (2014). Roles of F-box proteins in cancer. Nat. Rev. Cancer 14, 233–247. [PubMed: 24658274]

Wang ZA, Mitrofanova A, Bergren SK, Abate-Shen C, Cardiff RD, Califano A, and Shen MM (2013b). Lineage analysis of basal epithelial cells reveals their unexpected plasticity and supports a cell-of-origin model for prostate cancer heterogeneity. Nat. Cell Biol 15, 274–283. [PubMed: 23434823]

Wei S, Kozono S, Kats L, Nechama M, Li W, Guarnerio J, Luo M, You MH, Yao Y, Kondo A, et al. (2015). Active Pin1 is a key target of all-trans retinoic acid in acute promyelocytic leukemia and breast cancer. Nat. Med 21, 457–466. [PubMed: 25849135]

Wong OG, and Cheung AN (2016). Stem cell transcription factor NANOG in cancers–is eternal youth a curse? Expert Opin. Ther. Targets 20, 407–417.

Xu J, Mo Z, Ye D, Wang M, Liu F, Jin G, Xu C, Wang X, Shao Q, Chen Z, et al. (2012). Genome-wide association study in Chinese men identifies two new prostate cancer risk loci at 9q31.2 and 19q13.4. Nat. Genet 44, 1231–1235. [PubMed: 23023329]

Zheng N, Zhou Q, Wang Z, and Wei W (2016). Recent advances in SCF ubiquitin ligase complex: clinical implications. Biochim. Biophys. Acta 1866, 12–22. [PubMed: 27156687]

Zhou XZ, and Lu KP (2016). The isomerase PIN1 controls numerous cancer-driving pathways and is a unique drug target. Nat. Rev. Cancer 16, 463–478. [PubMed: 27256007]

Zhuang M, Calabrese MF, Liu J, Waddell MB, Nourse A, Hammel M, Miller DJ, Walden H, Duda DM, Seyedin SN, et al. (2009). Structures of SPOP-substrate complexes: insights into molecular architectures of BTB-Cul3 ubiquitin ligases. Mol. Cell 36, 39–50. [PubMed: 19818708]

Highlights

- SPOP promotes Nanog ubiquitination and degradation to suppress stem cell traits
- Cancer-associated SPOP mutants fail to promote Nanog destruction
- Cancer-derived mutation at Nanog-degron (S68Y) evades SPOP-mediated degradation
- Pin1 oncoprotein stabilizes Nanog through impairing its recognition by SPOP

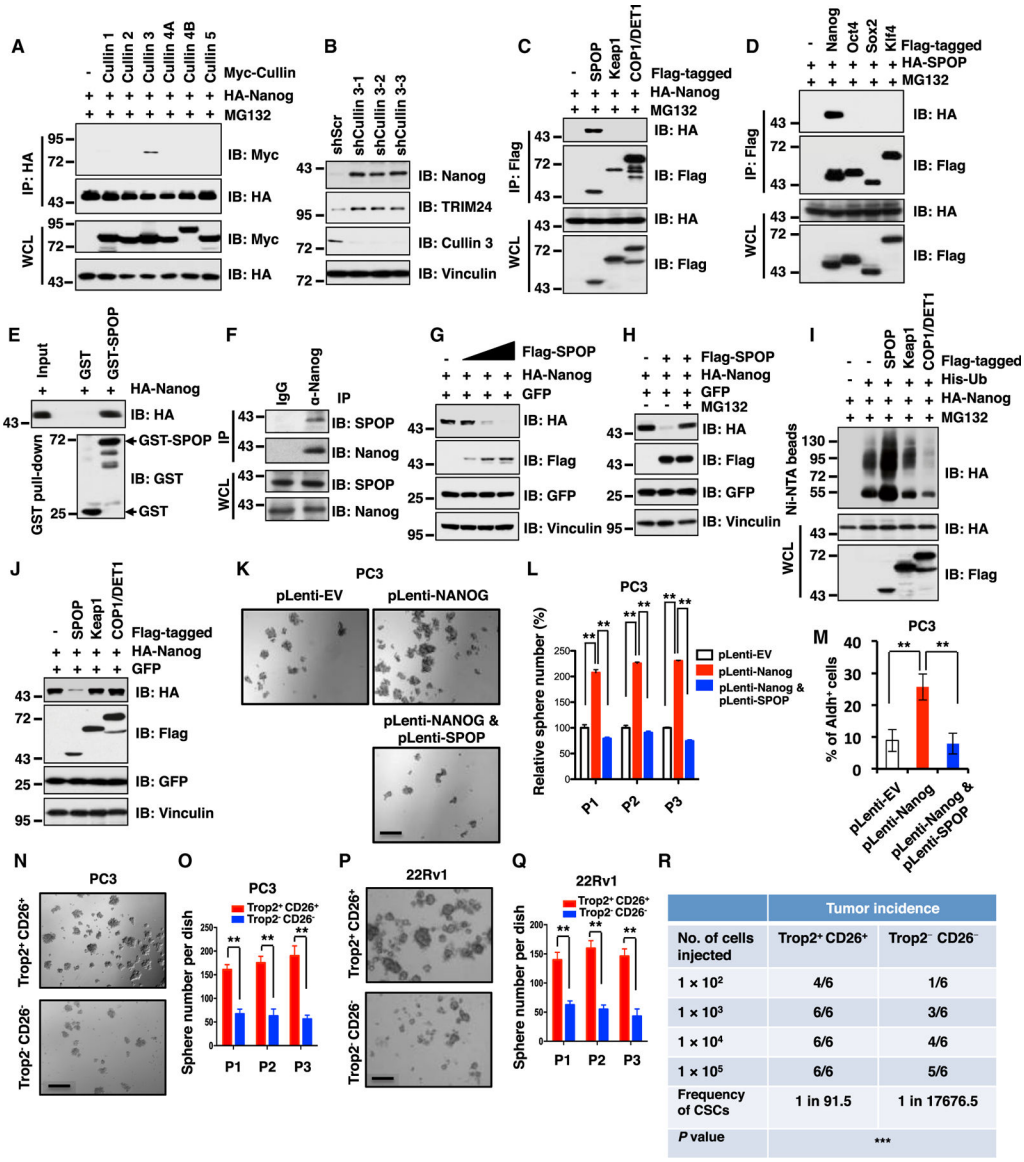

	Tumor incidence	
No. of cells injected	Trop2+ CD26+	Trop2− CD26−
1 × 10²	4/6	1/6
1 × 10³	6/6	3/6
1 × 10⁴	6/6	4/6
1 × 10⁵	6/6	5/6
Frequency of CSCs	1 in 91.5	1 in 17676.5
P value	***	

Figure 1. Cullin 3^{SPOP} Suppresses Prostate CSC Traits Largely through Promoting Nanog Poly-ubiquitination and Degradation

(A) Immunoblot (IB) analysis of whole-cell lysates (WCL) and immunoprecipitates (IP) derived from 293T cells transfected with indicated constructs. Cells were treated with MG132 (10 μM) for 12 hr before harvesting.

(B) IB analysis of WCL derived from PC3 cells infected with the indicated lentiviral shRNAs against *Cullin 3* and selected with puromycin (1 μg/mL) for 3 days before harvesting.

(C)IB analysis of WCL and anti-FLAG IP derived from 293T cells transfected with HA-Nanog, Flag-tagged SPOP, Keap1 or COP1/DET1 as indicated. Cells were treated with 10 μM MG132 for 12 h before harvesting.

(D) IB analysis of WCL and anti-Flag IP derived from 293T cells transfected with HA-SPOP, Flag-tagged Nanog, Oct4, Sox2 or Klf4 as indicated. Cells were treated with10 μM MG132 for 12 h before harvesting.

(E) IB analysis of glutathione S-transferase (GST) pull-down precipitates from 293T cell lysates with ectopic expression of hemagglutinin (HA)-Nanog incubated with bacterially purified recombinant GST or GST-SPOP protein.
(F) IB analysis of WCL and anti-Nanog IP derived from DU145 cells with indicated antibodies.
(G) IB analysis of WCL derived from 293T cells transfected with HA-Nanog, GFP or Flag-SPOP as indicated.
(H) IB analysis of WCL derived from 293T cells transfected with indicated constructs. Where indicated, cells were treated with 10 μM MG132 for 12 h before harvesting.
(I) IB of WCL and nickel-charged affinity resins (Ni-NTA) pull-down products derived from the lysates of PC3 cells transfected with the indicated constructs. Cells were treated with 30 μM MG132 for 6 hr before harvesting.
(J) IB analysis of WCL derived from 293T cells transfected with indicated constructs.
(K and L) PC3 cells stably expressing indicated constructs were analyzed by *in vitro* prostate sphere forming assays (see STAR Methods for details). Representative images (K) and quantification of sphere numbers at different passages (L) were shown.
(M) The aldehyde dehydrogenase activity positive ($Aldh^+$) cell population of PC3 cells stably expressing indicated constructs were measured through detecting Aldh enzymatic activity and analyzed by flow cytometry (see STAR Methods for details).
(N–Q) $Trop2^+CD26^+$ or $Trop2^-CD26^-$ PC3 or 22Rv1 cells were analyzed by *in vitro* prostate sphere forming assays. Representative images (N and P) and quantification of sphere numbers at different passages (O and Q) were shown.
(R) $Trop2^+CD26^+$ PC3 cells exhibited significantly higher tumor incidence than $Trop2^-CD26^-$ PC3 cells in a serial dilution xenograft assay. The frequency of cancer stem cells (CSCs) and the comparison of the difference between the two groups were calculated using ELDA (Extreme Limiting Dilution Analysis) online software (http://bioinf.wehi.edu.au/software/elda/). ***$p < 0.001$ (Chi-square test).
(K, N, and P) The scale bar represents 50 μm; (L, M, O, and Q) Data were presented as mean ± SD (n = 3). **$p < 0.01$ (t test).
See also Figure S1.

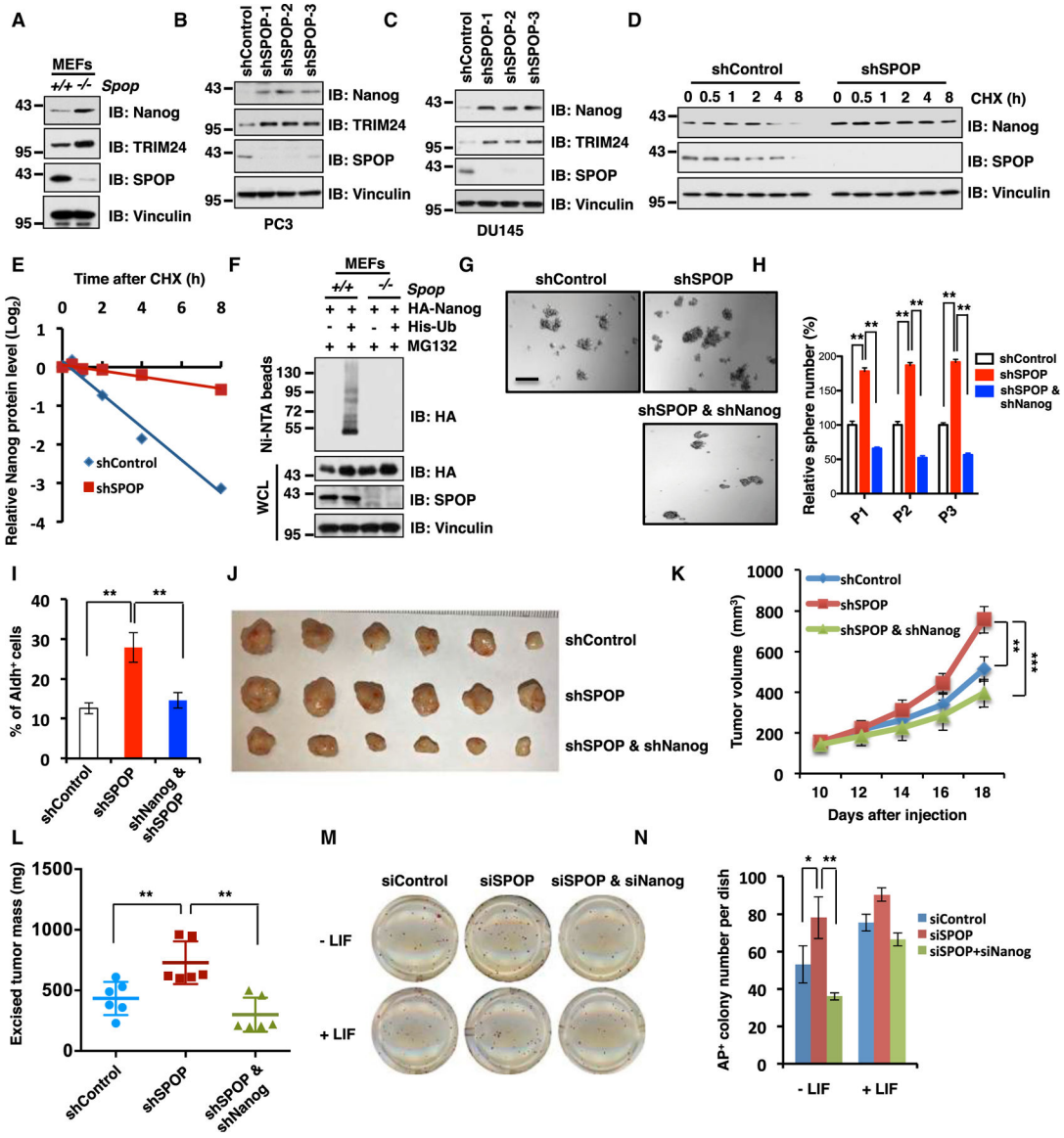

Figure 2. Depletion of *SPOP* Stabilizes Nanog to Promote Prostate Cancer Stem Cell Properties

(A) Immunoblot (IB) analysis of whole-cell lysates (WCLs) derived from *Spop*$^{+/+}$ and *Spop*$^{-/-}$ MEF cells with indicated antibodies.

(B) IB analysis of WCL derived from PC3 cells infected with indicated lentiviral shRNAs against *SPOP* and selected with puromycin (1 μg/ml) for 3 days before harvesting.

(C) IB analysis of WCL derived from DU145 cells infected with indicated lentiviral shRNAs against *SPOP* and selected with puromycin (1 μg/ml) for 3 days before harvesting.

(D and E) IB analysis of WCL derived from PC3 cells stably infected with lentiviral shRNAs transfected with indicated constructs. Cells were treated with 100 μg/mL cycloheximide (CHX) as indicated time points before harvesting. Nanog protein abundance in (D) was quantified by ImageJ and plotted in (E).

(F) IB of WCL and Ni-NTA pull-down products derived from the lysates of MEFs cells transfected with the indicated constructs. Cells were treated with 30 μM MG132 for 6 hr before harvesting.

(G and H) *In vitro* prostate sphere forming assays were performed for PC3 cells stably expressing indicated lentiviral shRNAs. Representative images (G) and quantification of sphere numbers at different passages (H) were shown. The scale bar represents 50 μm.

(I) The $Aldh^+$ cell population of PC3 cells stably infected with indicated lentiviral shRNAs was measured by detecting Aldh enzymatic activity and analyzed by flow cytometry (see STAR Methods for details).

(J–L) Tumor xenograft assays were performed with indicated PC3 stable cell lines. Tumors were dissected after euthanizing the mice, and tumor weights were recorded at the time of sacrifice (J and L). Tumor growth curves were based on measured tumor volume at different time points (K). Tumor dimensions were measured with calipers every two days, and the volume was calculated accordingly. Statistical analysis of tumor volumes at each time point showed significant differences in mean tumor volumes. $^{**}p < 0.01$, $^{***}p < 0.001$ (t test).

(M and N) Alkaline Phosphatase (AP) staining was used to quantify the percentage of pluripotent CJ7 embryonic stem (ES) cells after 72 hr transfection with indicated siRNAs. Representative images (M) and quantification of AP positive colony number (N) were shown.

(H, I and N) Data were presented as mean ± SD (n = 3). $^{**}p < 0.01$, $^{*}p < 0.05$ (t test).

(See also Figure S2.)

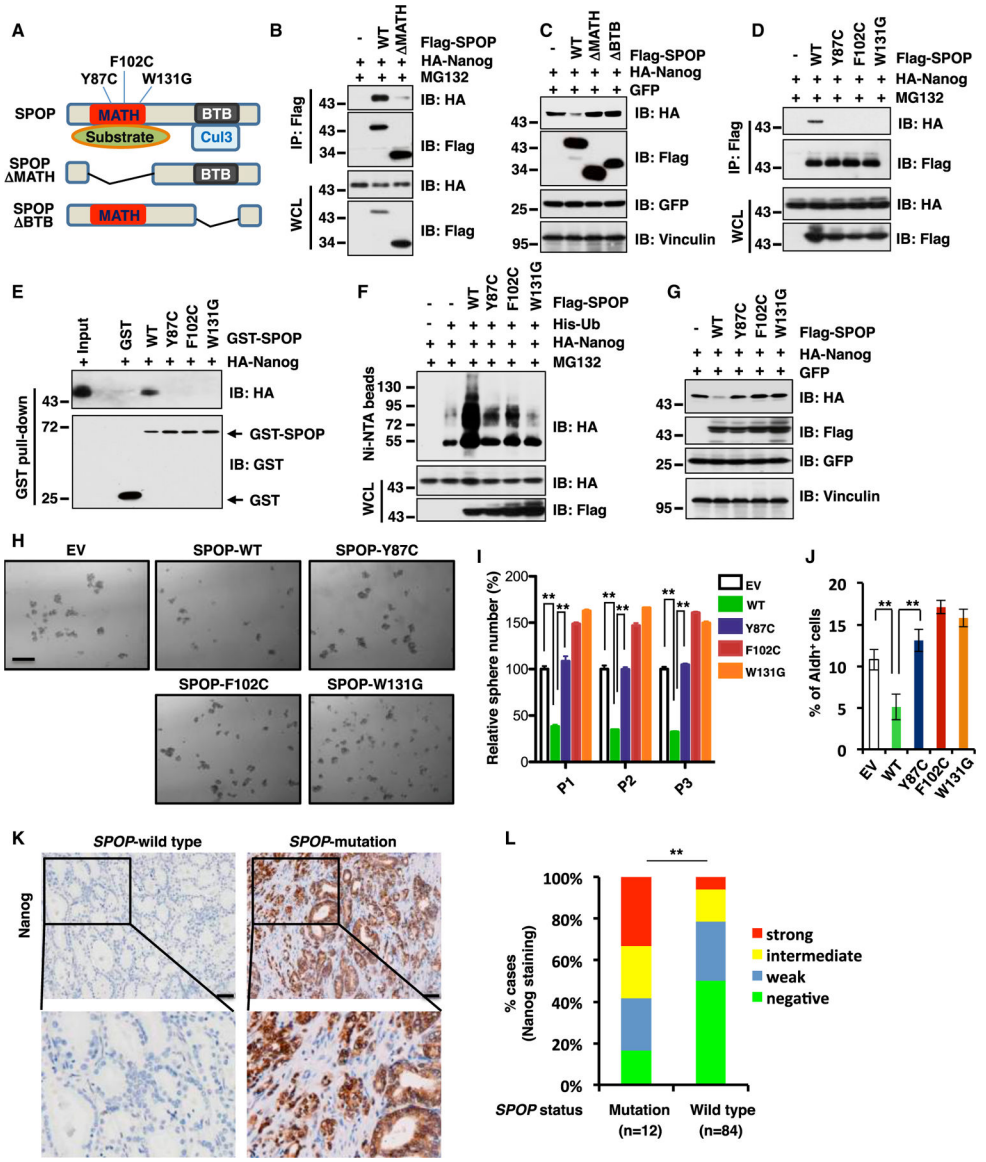

Figure 3. Prostate-Cancer-Associated SPOP Mutants Fail to Interact with Nanog to Promote Poly-ubiquitination and Subsequent Degradation of Nanog

(A) A schematic illustration of SPOP with MATH and BTB domain and prostate cancer-associated mutations.

(B) Immunoblot (IB) analysis of whole cell lysates (WCL) and anti-Flag IP derived from 293T cells transfected with HA-Nanog, Flag-SPOP WT or delta MATH mutant as indicated. Cells were treated with 10 μM MG132 for 12 h before harvesting.

(C) IB analysis of WCL derived from 293T cells transfected with indicated constructs.

(D) IB analysis of WCL and anti-Flag IP derived from 293T cells transfected with HA-Nanog, Flag-SPOP WT, Y87C, F102C or W131G mutant as indicated. Cells were treated with 10 μM MG132 for 12 h before harvesting.

(E) IB analysis of GST pull-down precipitates from 293T cell lysates with ectopic expression of HA-Nanog incubated with bacterially purified GST-SPOP WT and mutant recombinant proteins.

(F) IB of WCL and Ni-NTA pull-down products derived from the lysates of PC3 cells transfected with the indicated constructs. Cells were treated with 30 μM MG132 for 6 hr before harvesting.

(G) IB analysis of WCL derived from 293T cells transfected with indicated constructs.

(H and I) *In vitro* prostate sphere forming assays were performed for PC3 cells stably expressing indicated constructs. Representative images (H) and quantification of sphere numbers at different passages (I) were shown. The scale bar represents 50 μm. Data were presented as mean ± SD (n = 3). **p < 0.01 (t test).

(J) The $Aldh^+$ cell population of PC3 cells stably expressing indicated constructs was measured through detecting Aldh enzymatic activity and analyzed by flow cytometry. Data were presented as mean ± SD (n = 3). **p < 0.01 (t test).

(K and L) Representative images of Nanog immunohistochemical staining in *SPOP* wild-type or mutant primary prostate cancer samples (K) and quantification of Nanog expression levels in 84 cases of *SPOP* wild-type and 12 cases of *SPOP* mutation prostate tumor specimens (L) were shown. The scale bar represents 50 μm. **p < 0.01 (chi-square test). (See also Figure S3.)

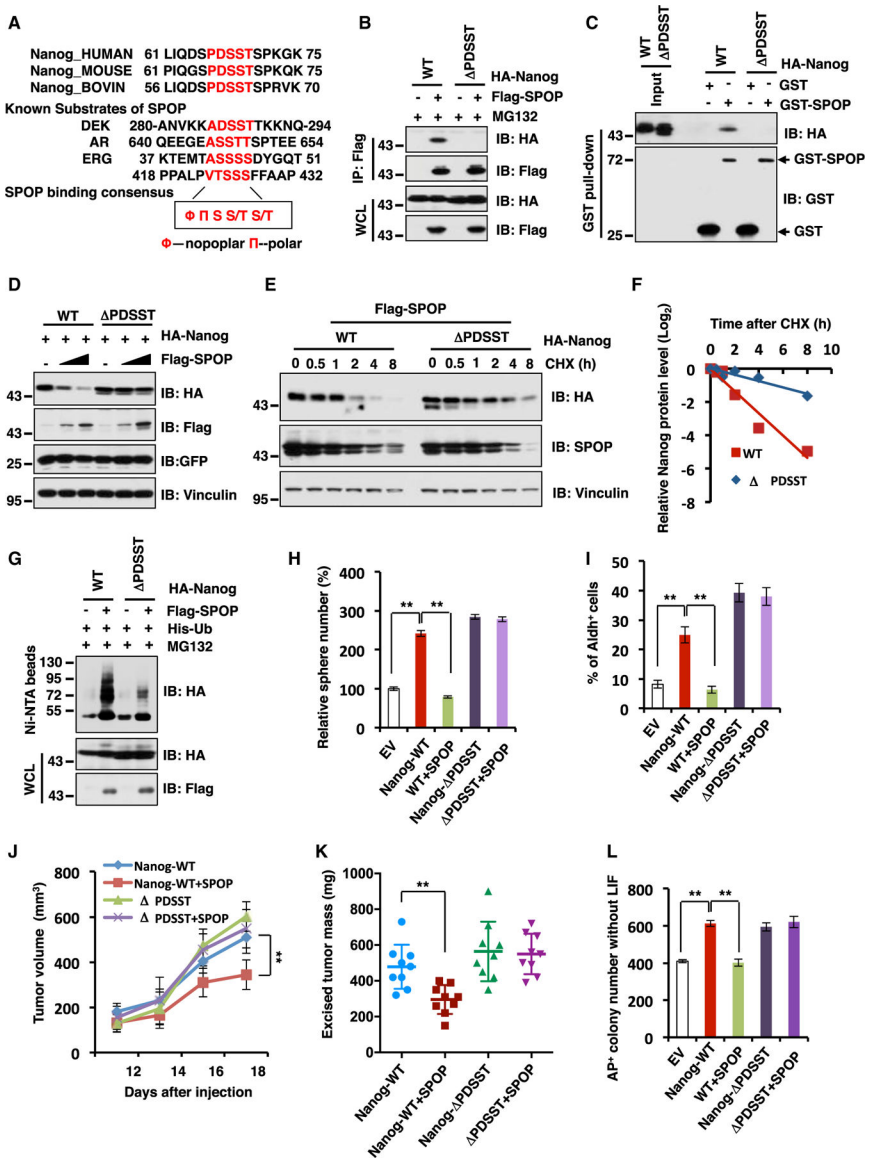

Figure 4. SPOP Promotes Nanog Poly-ubiquitination and Degradation in a Degron-Dependent Manner

(A) A sequence comparison of putative SPOP binding motif in Nanog with known SPOP substrates.

(B) Immunoblot (IB) analysis of whole-cell lysates (WCL) and anti-FLAG IP from 293T cells transfected with indicated constructs. Cells were treated with 10 μM MG132 for 12 hr before harvesting.

(C) IB analysis of GST pull-down products from 293T cell lysates with ectopic expression of HA-Nanog WT and deletion mutant (ΔPDSST) incubated with bacterially purified recombinant GST or GST-SPOP.

(D) IB analysis of WCL derived from 293T cells transfected with the indicated constructs.

(E and F) IB analysis of WCL derived from 293T cells transfected with indicated constructs. 36 hr post transfection, cells were treated with 100 μg/mL cycloheximide (CHX) as

indicated time points. Nanog WT and ΔPDSST protein abundance in (E) were quantified by ImageJ and plotted in (F), respectively.

(G) IB of WCL and Ni-NTA pull-down products derived from the lysates of PC3 cells transfected with the indicated constructs. Cells were treated with 30 μM MG132 for 6 hr before harvesting.

(H) The quantification of *in vitro* prostate sphere forming assays for Figure S4K was shown. Data were presented as mean ± SD (n = 3). **p < 0.01 (t test).

(I) The $Aldh^+$ cell population of PC3 cells stably expressing indicated constructs were measured through detecting Aldh enzymatic activity and analyzed by flow cytometry. Data were presented as mean ± SD (n = 3). **p < 0.01 (t test).

(J and K) Tumor xenograft mouse assays were performed with the cell lines generated in Figure S4J. Tumor growth curves were based on measured tumor volumes at different time points (J). Tumor dimensions were measured with calipers every two days, and the volume was calculated accordingly. Statistical analysis of tumor volumes at each time point showed significant differences in mean tumor volumes between the Nanog-WT and the Nanog-WT/SPOP groups. Tumors were dissected after euthanizing the mice, and tumor weights were recorded at the time of sacrifice (K).

(L) AP staining was used to quantify the percentage of pluripotent CJ7 ES cells after 72 hr transfection with indicated constructs. The quantification of AP positive colony number was shown. Data were presented as mean ± SD (n = 3). **p < 0.01 (t test).

(See also Figure S4.)

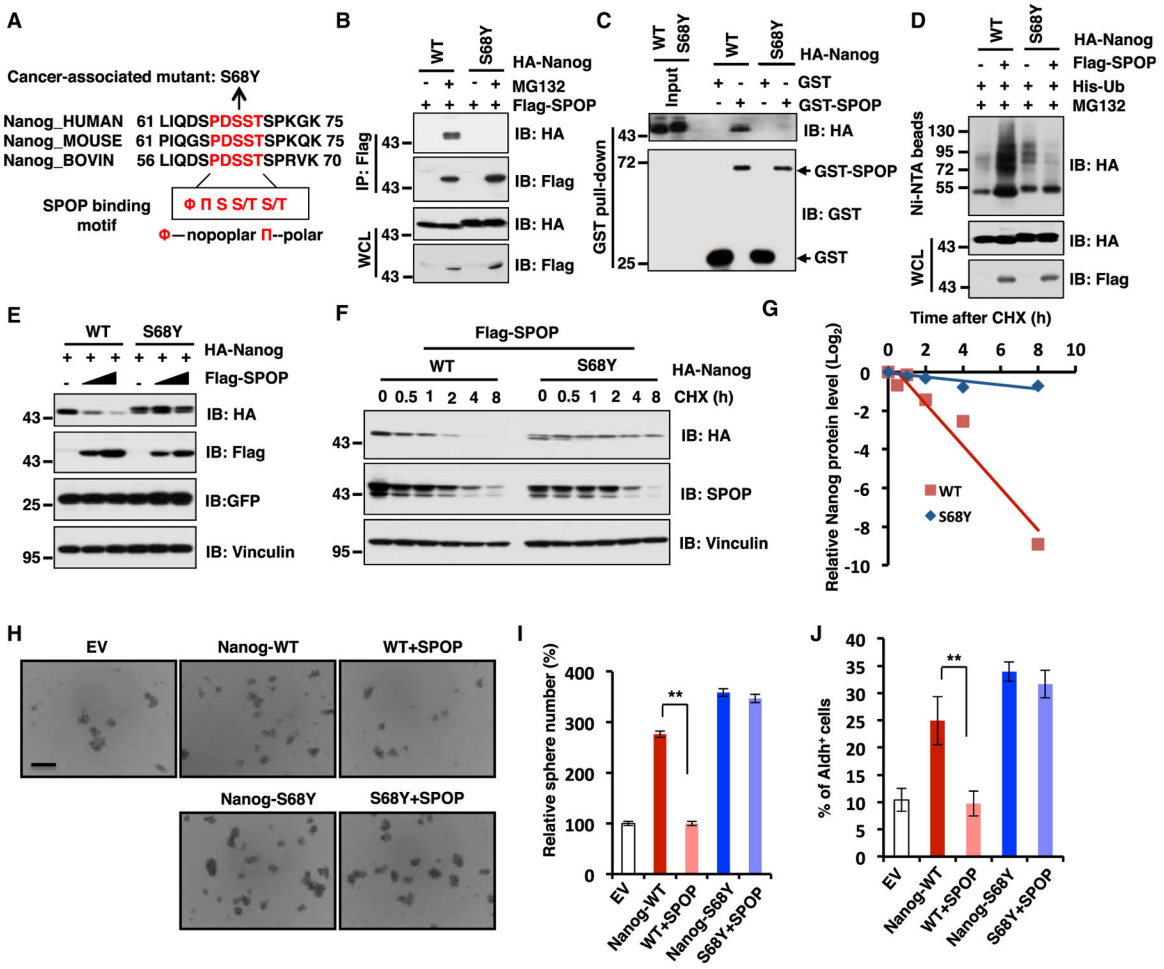

Figure 5. Cancer-Patient-Derived Nanog Mutation (S68Y) in the Degron Motif Confers Resistance to SPOP-Mediated Destruction of Nanog

(A) A sequence comparison of SPOP binding motif in Nanog derived from different species.

(B) Immunoblot (IB) analysis of whole-cell lysates (WCLs) and anti-FLAG IP from 293T cells transfected with indicated constructs and were treated with 10 μM MG132 for 12 hr before harvesting.

(C) IB analysis of GST pull-down products from 293T cell lysates with ectopic expression of HA-Nanog WT and deletion mutant (S68Y) incubated with bacterially purified GST or GST-SPOP.

(D) IB of WCL and Ni-NTA pull-down products derived from the lysates of PC3 cells transfected with the indicated constructs and were treated with 30 μM MG132 for 6 hr before harvesting.

(E) IB analysis of WCL derived from 293T cells transfected with the indicated constructs.

(F and G) IB analysis of WCL derived from 293T cells transfected with indicated constructs. 36 hr post transfection, cells were treated with 100 μg/mL cycloheximide (CHX) as indicated time points. Nanog WT and S68Y protein abundance in (F) were quantified by ImageJ and plotted in (G), respectively.

(H and I) *In vitro* prostate sphere forming assays were performed for PC3 cells stably cell lines generated in Figure S5H. Representative images (H) and quantification of sphere

numbers at different passages (I) were shown. The scale bar represents 50 mm. Data were presented as mean ± SD (n = 3). **p < 0.01 (t test).

(J) The $Aldh^+$ cell population of PC3 cells stably expressing indicated constructs was measured through detecting Aldh enzymatic activity and analyzed by flow cytometry. Data were presented as mean ± SD (n = 3). **p < 0.01 (t test).

See also Figure S5.

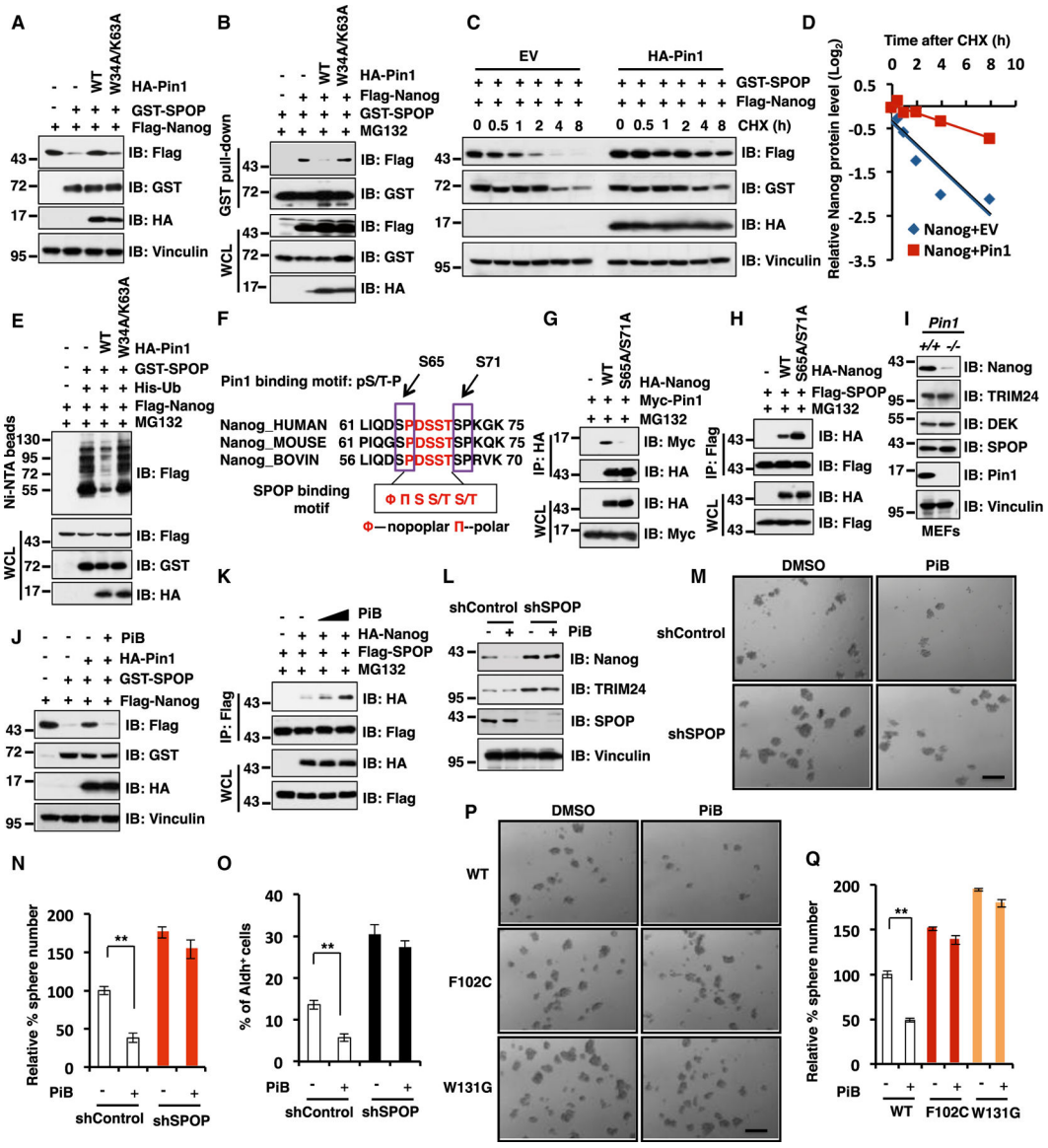

Figure 6. The Pin1 Inhibitors Promote SPOP-Mediated Destruction of Nanog to Suppress Prostate Cancer Stem Cell Traits

(A) Immunoblot (IB) analysis of whole-cell lysates (WCLs) from 293T cells transfected with indicated constructs.

(B) IB analyses of WCL and GST pull-down products from 293T cells transfected with indicated constructs and treated with 10 μM MG132 for 12 hr before harvesting.

(C and D) IB analysis of WCL derived from 293T cells transfected with indicated constructs. 36 hr post transfection, cells were treated with 100 μg/mL cycloheximide (CHX) as indicated time points. Nanog protein abundance in (C) was quantified by ImageJ and plotted in (D), respectively.

(E) IB of WCL and Ni-NTA pull-down products derived from the lysates of PC3 cells transfected with the indicated constructs. Cells were treated with 30 μM MG132 for 6 hr before harvesting.

(F) A schematic illustration of sequence comparison for the SPOP binding motif in Nanog from different species to show the two conservative SP sites as putative Pin1 interacting site(s).

(G and H) IB analyses of WCL and anti-HA (G) or anti-FLAG (H) immunoprecipitations from 293T cells transfected with indicated constructs and treated with 10 μM MG132 for 12 hr before harvesting.

(I) IB analysis of WCL derived from *Pin1*$^{+/+}$ and *Pin1*$^{-/-}$ MEF cells with indicated antibodies.

(J) IB analyses of WCL from 293T cells transfected with indicated constructs and treated with the Pin1 inhibitor (PiB, 20 μM) for 8 hr before harvesting.

(K) IB analyses of WCL and anti-FLAG immunoprecipitations from 293T cells transfected with indicated constructs and were treated with MG132 (10 μM) for 12 hr and the Pin1 inhibitor, PiB, (10 or 20 μM) for 8 hr before harvesting.

(L) IB analyses of WCL derived from PC3 cells stably expressing shControl or shSPOP with or without PiB (20 μM) treatment for 8 hr before harvesting.

(M and N) *In vitro* prostate sphere forming assays were performed for PC3 cells stably expressing shControl or shSPOP in the presence or absence of PiB. Representative images (M) and quantification of sphere numbers at different passages (N) were shown. The scale bar represents 50 μm. Data were presented as mean ± SD (n = 3). **p < 0.001 (t test).

(O) PC3 cells stably expressing indicated constructs were treated with Pin1 inhibitor (PiB, 2 μM) for 3 days. Subsequently, cells were measured through detecting Aldh enzymatic activity and analyzed by flow cytometry. Data were presented as mean ± SD (n = 3). **p < 0.001 (t test).

(P and Q) *In vitro* prostate sphere forming assays were performed for PC3 cells stably expressing SPOP-WT, F102C, or W131G SPOP-mutants in the presence or absence of the Pin1 inhibitor, PiB. Representative images (P) and quantification of sphere numbers at different passages (Q) were shown. The scale bar represents 50 μm. Data were presented as mean ± SD (n = 3). **p < 0.001 (t test).

See also Figure S6.